Mutations in *MAPKBP1* Cause Juvenile or Late-Onset Cilia-Independent Nephronophthisis

Maxence S. Macia,[1,2] Jan Halbritter,[3,4,22] Marion Delous,[1,2,22] Cecilie Bredrup,[5,6] Arthur Gutter,[1,2] Emilie Filhol,[1,2] Anne E.C. Mellgren,[5,6,7] Sabine Leh,[7,8] Albane Bizet,[1,2] Daniela A. Braun,[3] Heon Y. Gee,[3] Flora Silbermann,[1,2] Charline Henry,[1,2] Pauline Krug,[1,2,9] Christine Bole-Feysot,[2,10] Patrick Nitschké,[2,11] Dominique Joly,[12] Philippe Nicoud,[13] André Paget,[13] Heidi Haugland,[14] Damien Brackmann,[15] Nayir Ahmet,[16] Richard Sandford,[17] Nurcan Cengiz,[18] Per M. Knappskog,[6,19] Helge Boman,[6] Bolan Linghu,[20] Fan Yang,[20] Edward J. Oakeley,[21] Pierre Saint Mézard,[21] Andreas W. Sailer,[21] Stefan Johansson,[6,19] Eyvind Rødahl,[5,7,23] Sophie Saunier,[1,2,23,*] Friedhelm Hildebrandt,[3,23,*] and Alexandre Benmerah[1,2,23]

Nephronophthisis (NPH), an autosomal-recessive tubulointerstitial nephritis, is the most common cause of hereditary end-stage renal disease in the first three decades of life. Since most NPH gene products (NPHP) function at the primary cilium, NPH is classified as a ciliopathy. We identified mutations in a candidate gene in eight individuals from five families presenting late-onset NPH with massive renal fibrosis. This gene encodes MAPKBP1, a poorly characterized scaffolding protein for JNK signaling. Immunofluorescence analyses showed that MAPKBP1 is not present at the primary cilium and that fibroblasts from affected individuals did not display ciliogenesis defects, indicating that MAPKBP1 may represent a new family of NPHP not involved in cilia-associated functions. Instead, MAPKBP1 is recruited to mitotic spindle poles (MSPs) during the early phases of mitosis where it colocalizes with its paralog WDR62, which plays a key role at MSP. Detected mutations compromise recruitment of MAPKBP1 to the MSP and/or its interaction with JNK2 or WDR62. Additionally, we show increased DNA damage response signaling in fibroblasts from affected individuals and upon knockdown of *Mapkbp1* in murine cell lines, a phenotype previously associated with NPH. In conclusion, we identified mutations in *MAPKBP1* as a genetic cause of juvenile or late-onset and cilia-independent NPH.

Nephronophthisis (NPH [MIM: 256100]) is an autosomal-recessive kidney disorder characterized by the development of massive interstitial fibrosis with abnormal thickness of the tubular basement membranes, atrophic and/or dilated tubules, and occasionally, formation of cysts mainly distributed at the cortico-medullary junction within normal sized or small kidneys. It is the main genetic cause of end-stage renal disease (ESRD) in the first two decades of life and three different forms have been clinically described based on the mean age at ESRD: infantile (<3 years), juvenile (mean 13 years), and late onset (mean 19 years).[1]

NPH can be either isolated or associated with different extra-renal manifestations (retinal dystrophy, liver fibrosis, skeleton dysplasia, etc.) in syndromic forms referred to hereafter as nephronophthisis-related ciliopathies (NPH-RCs). Indeed, the great majority of the 20 genes associated with NPH-RCs encode proteins (NPHP) that localize to primary cilia where they play key functions in the biogenesis of this organelle as well as in cilia-dependent signaling pathways.[1–3] NPH has therefore been classified as a ciliopathy, in a growing family of genetic diseases linked to either primary and/or motile cilia dysfunctions.[4] In addition, recent evidence established that NPH-RCs can also be linked to the DNA damage response (DDR) signaling pathway. Initially identified for *NPHP14/ZNF423* (MIM: 614844) and *NPHP15/CEP164* (MIM: 614848),[5] enhanced DDR signaling was also associated with mutations in several other *NPHP* genes evidenced by mouse models of *NPHP6/CEP290*[6] (MIM: 610142), *NPHP9/NEK8*[7,8] (MIM: 613824), and *NPHP10/SDCCAG8*[9] (MIM: 613524). Altogether, these data suggest that increased DDR signaling may underlie progressive renal disease seen in NPH[10] as well as a possible functional link between cilia and regulation of DDR signaling which remains to be uncovered. Except for

[1]INSERM, UMR-1163, Laboratory of Inherited Kidney Diseases, 75015 Paris, France; [2]Paris Descartes - Sorbonne Paris Cité University, Imagine Institute, 75015 Paris, France; [3]Division of Nephrology, Department of Medicine, Boston Children's Hospital, Harvard Medical School, Boston, MA 02115, USA; [4]Division of Nephrology, Department of Internal Medicine, University Clinic Leipzig, 04103 Leipzig, Germany; [5]Department of Ophthalmology, Haukeland University Hospital, 5021 Bergen, Norway; [6]Center for Medical Genetics and Molecular Medicine, Haukeland University Hospital, 5021 Bergen, Norway; [7]Department of Clinical Medicine, University of Bergen, 5021 Bergen, Norway; [8]Department of Pathology, Haukeland University Hospital, 5021 Bergen, Norway; [9]Pediatric Nephrology Department, Necker-Enfants Malades Hospital, 75015 Paris, France; [10]Inserm UMR-1163, Genomic Core Facility, 75015 Paris, France; [11]Paris Descartes - Sorbonne Paris Cité University, Bioinformatics Core Facility, 75015 Paris, France; [12]Nephrology Department, Necker -Enfants Malades Hospital, 75015 Paris, France; [13]Hemodialysis-Nephrology Department, Mont-Blanc Hospitals, 74700 Sallanches, France; [14]Department of Ophthalmology, Førde Central Hospital, 6812 Førde, Norway; [15]Department of Pediatrics, Haukeland University Hospital, 5021 Bergen, Norway; [16]University of Istanbul, 34452 Istanbul, Turkey; [17]Academic Department of Medical Genetics, University of Cambridge, CB2 0QQ Cambridge, UK; [18]Baskent University, 06810 Ankara, Turkey; [19]Department of Clinical Science, University of Bergen, 5021 Bergen, Norway; [20]Novartis Institutes for Biomedical Research, Cambridge, MA 02139, USA; [21]Novartis Institutes for Biomedical Research, 4002 Basel, Switzerland
[22]These authors contributed equally to this work
[23]These authors contributed equally to this work
*Correspondence: sophie.saunier@inserm.fr (S.S.), friedhelm.hildebrandt@childrens.harvard.edu (F.H.)
http://dx.doi.org/10.1016/j.ajhg.2016.12.011.

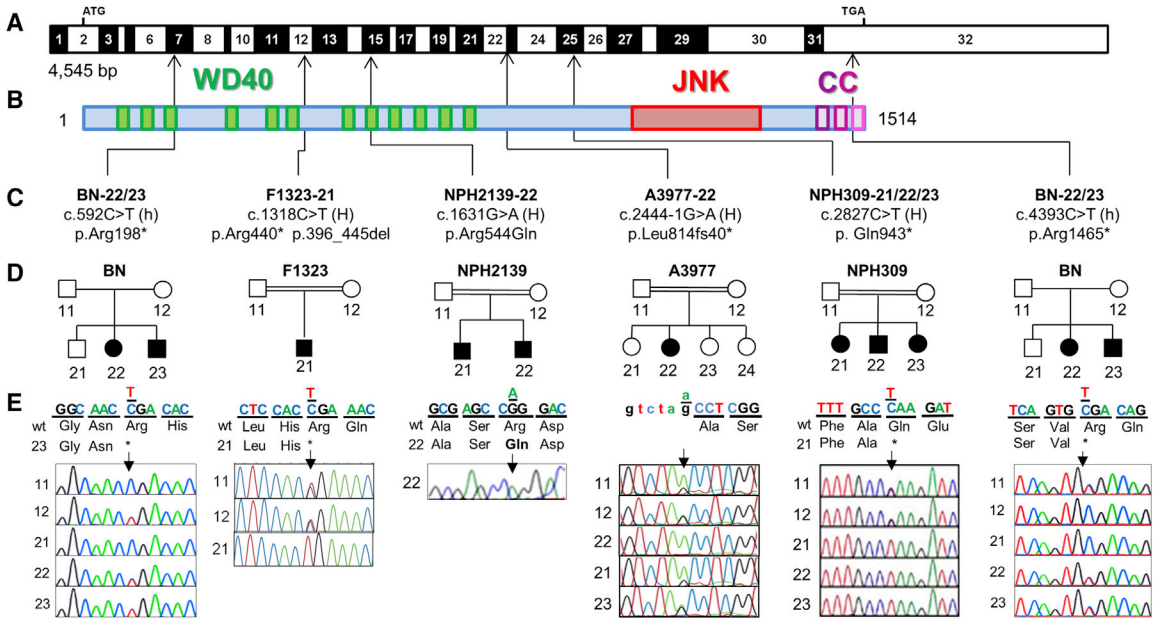

Figure 1. Biallelic Mutations in *MAPKBP1* Cause Nephronophthisis
(A) Exon structure of *MAPKBP1* cDNA. Positions of start codon (ATG) and stop codon (TGA) are indicated.
(B) Domain structure of the protein. MAPKBP1 contains 12 WD repeats (green), located at the N terminus, a JNK-binding region located in the C-terminal part (red), and conserved coiled-coil domains at the C terminus (CC, purple).
(C) Relation of four homozygous (H) and two compound heterozygous mutations (h) to exons and protein domains is indicated by black arrows.
(D and E) Pedigrees (D) and chromatograms and segregation (E). Mutated nucleotides are shown above wild-type. In addition, individuals BN-21 and BN-23 also presented with retinitis pigmentosa (RP) linked to a homozygous mutation in *PDE6A*.
See Figure S5. Segregation of the *MAPKBP1* mutations was not examined in family NPH2139 due to the unavailability of the DNA of the affected brother and the parents.

ZNF423 (MIM: 604557), which was not implicated in direct ciliary function, all NPHPs that have been involved in DDR signaling do also play a crucial role at primary cilia.[1,10]

In order to identify additional genes mutated in NPH, we independently performed homozygosity mapping and/or whole-exome sequencing (WES) on affected individuals from our cohorts (Figure S1, Table S1). Blood samples and pedigrees were obtained from individuals with diagnosed NPH-RCs. Written informed consent was obtained from all individuals enrolled in this study and/or from parents and approved by the Comité de Protection des Personnes pour la Recherche Biomédicale Ile de France II, the Institutional Review Board (IRB) at the Boston Children's Hospital (Boston), or the Regional Committee for Medical and Research Ethics, Western Norway (IRB no. 00001872). Affected individuals were included in WES upon either parental consanguinity or as member of a multiplex family. In total, WES was performed in 141 families, 85 with isolated NPH and 56 with syndromic NPH. Compound heterozygous nonsense (c.592C>T [p.Arg198*]; c.4393C>T [p.Arg1465*] in BN-23), homozygous nonsense (c.1318C>T [p.Arg440*] in F1323-21; c.2827C>T [p.Gln943*] in NPH309-21), as well as homozygous splice site mutations (c.2444−1G>A [p.Leu814fs40*] in A3977-22) were identified in *MAPKBP1* (GenBank: NM_001128608.1) in four affected individuals from four independent families (Figure 1 and Table 1). Additional competing biallelic missense variants were detected, but none of them are thought to possess an equally strong impact on the protein level, for either mild in silico prediction, occurrence in SNP databases (e.g., ExAC), or little evolutionary amino acid conservation (Table S2).

Additional screening of 342 unrelated affected individuals (108 with isolated NPH and 234 with syndromic NPH) using targeted exome sequencing[2,11] led to the identification in an affected individual (NPH2139-22) presenting late-onset isolated NPH of a homozygous missense variant (c.1631G>A [p.Arg544Gln]) never reported in ExAC database and predicted as damaging (PolyPhen-2 score, 1; SIFT, deleterious/score: 0; MutationTaster, disease causing). Interestingly, the Arg544 is part of a stretch of 12 aa that is highly conserved (almost identical) in both MAPKBP1 and WDR62 proteins from humans to *Drosophila* (Figure S2A). Furthermore, 3D structure analysis on equivalent residues in other WD40 domain-containing proteins indicates that Arg544 is located in a conserved site involved in the interaction of the WD40 domain with its partner(s) (Figures S2B and S2C), suggesting that the p.Arg544Gln variation may alter the binding of MAPKBP1 with potential and not yet identified partners.

Segregation of the identified mutations could be examined by Sanger sequencing for all the families except NPH2139. It showed that parents and unaffected siblings were heterozygous for the identified mutations (BN,

Table 1. Mutations of *MAPKBP1* in Five Families with Nephronophthisis

Individuals	Ethnic Origin	Nucleotide Alterations[a]	Deduced Protein Change	Exon, Zygosity	Parental Consanguinity	ESRD Years	RTX Years	Extrarenal Clinical Features
BN-22	Norway	c.592C>T, c.4393C>T	p.Arg198*, p.Arg1465*	7, 32, Het	no	no (25)	–	loose patella, long fingers and feet
BN-23	Norway	c.592C>T, c.4393C>T	p.Arg198*, p.Arg1465*	7, 32, Het	no	no (27)	–	RP,[b] CHD, severe meningomyelocele, statural growth delay
F1323-21	Turkey	c.1318C>T[c], exon 12 skipping	p.Arg440*, p.396_445del	12, Hom	yes	12	15	facial dysmorphism
NPH2139-22	Portugal	c.1631G>A	p.Arg544Gln[d]	15, Hom	yes	no (23)	–	none
A3977-22	Turkey	c.2444-1G>A, 5′ splice site	5′ splice site	22, Hom	yes	15	–	short stature
NPH309-21	Italy	c.2827C>T	p.Gln943*	25, Hom	yes	22	22,39	scoliosis
NPH309-22	Italy	c.2827C>T	p.Gln943*	25, Hom	yes	25	27,38	scoliosis, vesiculo-ureteral reflux, cholesteatoma, amyloid angiopathy
NPH309-23	Italy	c.2827C>T	p.Gln943*	25, Hom	yes	20	21	scoliosis, mild mental retardation, short stature, palate cleft

Abbreviations are as follows: ESRD, end-stage renal disease; CHD, congenital heart disease; Het, heterozygous; Hom, homozygous; NPH, nephronophthisis; RP, retinitis pigmentosa; RTX, renal transplantation.
[a]cDNA mutations are numbered according to human cDNA reference sequence GenBank: NM_001128608.1, isoform b (*MAPKBP1*), where +1 corresponds to the A of ATG start translation codon.
[b]Individuals BN-23 and BN-21 also present with RP linked to homozygous mutation in *PDE6A* (Figure S5).
[c]rs202001274: variant is listed in ExAC database, 2 of 121,258 are heterozygote. None of the others are currently listed.
[d]PolyPhen-2 score, 1; MutationTaster, disease causing; SIFT deleterious/score: 0.

F1323, NPH309, A3977) and that affected siblings were also presenting corresponding biallelic mutations in *MAPKBP1* (BN, NPH309; Figure 1 and Table 1). We consequently identified mutations in *MAPKBP1* in eight individuals from five families. They almost all presented with late-onset NPH (ESRD from 15 to >27 years) or juvenile NPH (for individual F1323-21 who presented ESRD at 12 years) (Table 1). Renal biopsies and ultrasounds from affected individuals (Figure 2) showed classical features of NPH characterized by atrophic tubules with thickening of the basement membranes, massive interstitial fibrosis, as well as the presence of interstitial infiltrate (BN-23 shown in Figure 2A, panels 1 and 2; NPH2139-21 shown in Figure 2C, panel 2; A3977-22 shown in Figure 2D, panel 1) as well as increased echogenicity and cysts (Figure 2D, panels 2 and 3).

Among the three nonsense mutations, the homozygous c.1318C>T (p.Arg440*) mutation in individual F1323-21 was investigated more closely. Indeed, in silico analysis of MAPKBP1 transcripts revealed an alternative splicing leading to the skipping of exon 12 (NCBI; GenBank: XM_011521383.1). This alternative transcript is predicted to lead to an in-frame deletion and a 1,475 amino acid protein (versus 1,514 for full-length MAPKBP1). Because c.1318C>T (p.Arg440*) was located in the exon 12 (Figure S3A), we next analyzed the expression and ratio of the various transcripts in individual F1323-21. Amplification of the exon 11–13 region by RT-PCR from F1323-21 fibroblasts revealed the presence of two products: one product also detected in the unrelated affected and control individuals (BN-22 and BN-12) and a shorter product (Figure S3B). Sanger sequencing analysis confirmed that the longer product corresponds to the full-length exon 12 containing transcript presenting the c.1318C>T nonsense mutation while the shorter band corresponds to a transcript that effectively lacks exon 12 (Figures S2B and S2C). The high amount of transcript lacking exon 12 in individual F1323-21 may possibly be explained by the fact that the c.1318C>T mutation is predicted to affect the binding of serine-arginine-rich protein SF2/ASF to putative exonic splicing enhancers (ESEfinder 3.0;[12] Figures S4A and S4B), which is then expected to affect the recruitment of splicing factors to splice sites and to lead to the skipping of exon 12 (Figure S4C). Skipping of exon 12 results in an in-frame deletion of 49 amino acids (aa 396 to 445) encompassing the sixth WD repeat out of the seven predicted to form a WD domain (Figure S3D). The resulting Δexon12 V5-tagged construct was poorly expressed upon transient transfection, with a migration profile in western blot experiments different from what was expected (Figure S3E, arrow), suggesting that the lack of exon 12 likely leads to misfolding of the N-terminal WD domain and decreased stability of the resulting protein. In conclusion, individual F1323-21 expressed two *MAPKPB1* transcripts, one coding for the expected p.Arg440* protein and a shorter spliced form lacking exon 12, both of these proteins being likely non- or poorly functional (see below).

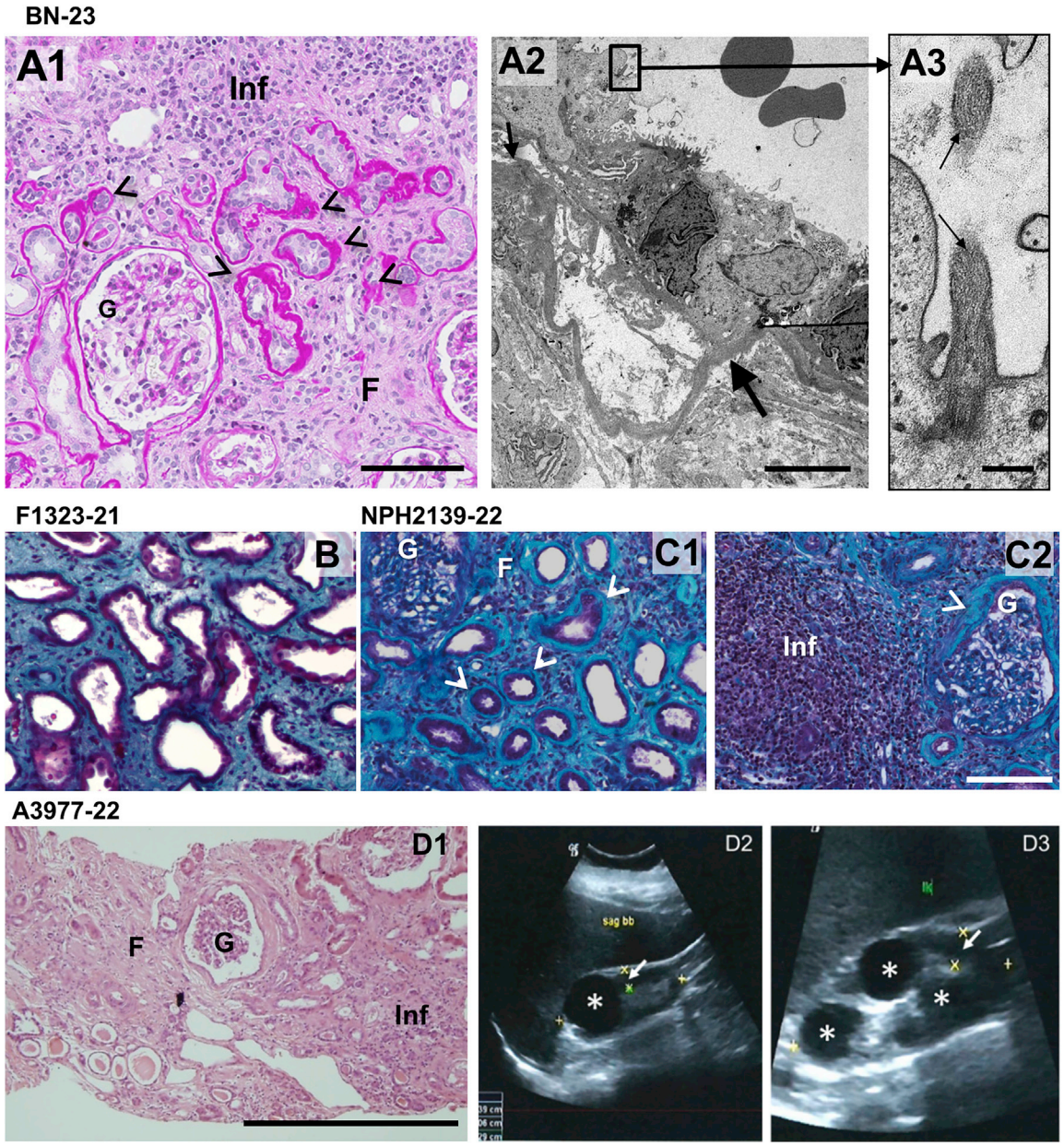

Figure 2. Histological and Sonographic Kidney Lesions in Individuals with *MAPKBP1* Mutations
(A1) Periodic acid-Schiff staining of a kidney biopsy from individual BN-23 showing tubular atrophy (arrowheads), interstitial fibrosis (F), focal interstitial infiltration (Inf), and normal glomerulus (G). Scale bar represents 100 μm.
(A2) Ultrastructure (transmission electron microscopy picture) from a tubule with abrupt transition from thin to thickened and disorganized basement membrane (arrow). Scale bar represents 5 μm.
(A3) Example of a primary cilium found at the apical membrane of a tubular epithelial cell (arrows). Scale bar represents 250 μm.
(B) Trichrome staining of a kidney biopsy from individual F1323-21 showing fibrosis, thickened basal membrane, as well as atrophic and dilated tubules.
(C) PAS trichrome staining of a kidney biopsy from individual NPH2139-21 showing tubular atrophy (arrowheads in C1), interstitial fibrosis (F) and focal interstitial infiltration (Inf, C2), and sclerotic glomeruli (G, C2) surrounded by a thickened capsular basement membrane (arrows, C1 and C2). Scale bar represents 100 μm.
(D1) Histological analysis of individual A3977-22 shows massive interstitial fibrosis and atrophic tubules. Scale bar represents 100 μm.
(D2 and D3) Upon renal ultrasound, kidneys present small with narrowed parenchyma (white arrow), increased echogenicity, and single cysts on both sides (white asterisk). D2 right kidney, D3 left kidney.

NPH in the affected individuals was not associated with other classically found extra-renal manifestations of NPHRCs, except retinitis pigmentosa (RP [MIM: 613810]) found in two out of three siblings of the BN family, suggesting Senior-Loken syndrome (SLS).[1] However, only individual BN-23 presented with both RP and NPH whereas his siblings presented with either NPH (BN-22) or RP (BN-21). Interestingly, while *MAPKBP1* mutations segregated only with NPH but not with RP, WES of individual BN-23 revealed the co-occurrence of a homozygous mutation in

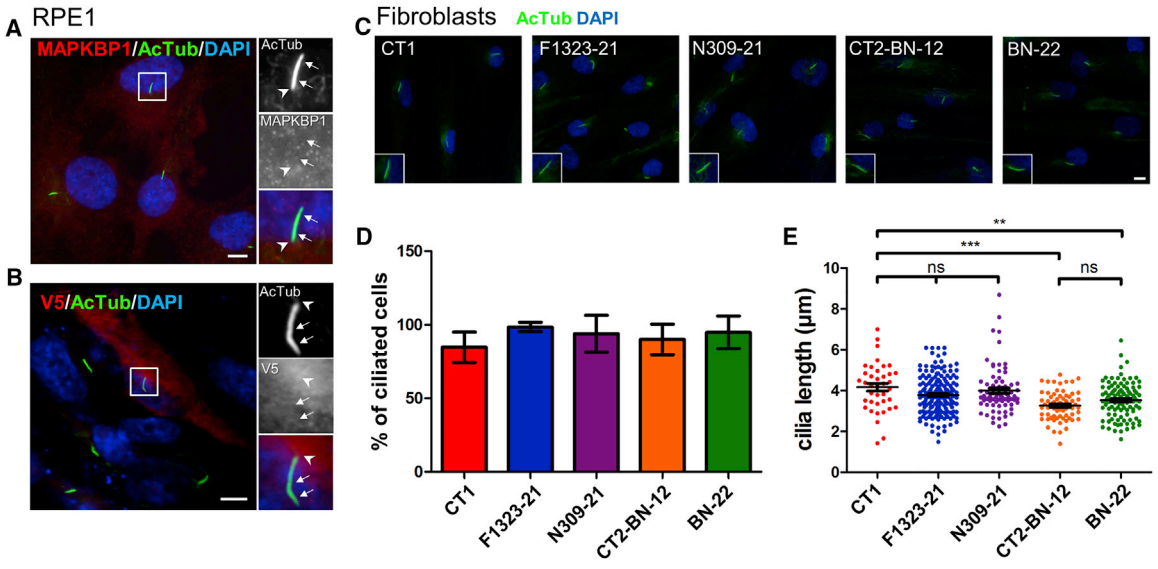

Figure 3. MAPKBP1 Is Not Involved in Ciliogenesis

(A and B) Serum-starved (24 hr) nontransfected RPE1 cells (A) or RPE1 cells transiently transfected (FuGENE [Promega]) with V5-tagged MAPKBP1 encoding plasmid (B) were fixed (paraformaldehyde; PFA) and stained for acetylated α-tubulin (AcTub, green, cilia; mouse monoclonal antibody [6-11-B-1, Sigma], dil 1/10,000) and for endogenous MAPKBP1 (A) (red; rabbit polyclonal [HPA030832, Sigma], dil 1/300) or overexpressed MAPKBP1 (B) (red, V5 rabbit polyclonal antibody [Sigma V8137], dil 1/10,000). Insets on the right show higher magnifications of representative cilia indicated by a white square in the corresponding images. Arrows indicate cilia, arrowheads cilium base region.

(C–E) Serum-starved fibroblasts from controls (CT1 [unrelated healthy], CT2-BN-12 [mother of BN-22, heterozygous for the c.592C>T (p.Arg198*) mutation]) or from the affected individuals (BN-22, F1323-21, NPH309-21) were stained for acetylated-tubulin (AcTub, green) to identify cilia (C). Insets on the right show higher magnifications of representative cilia. Ciliogenesis (% of ciliated cells [D]) and length of cilia (E) were analyzed and quantified by ImageJ from three independent experiments ($n > 50$ cells for each experiment). ns,*$p < 0.01$, and ***$p < 0.0001$ were calculated via Dunn's multiple comparison test after the analysis of variance ANOVA test. Note that cilia length in cells from individual BN-22 is not significantly different from that of cilia from cells of his mother (CT2-BN-12). Cilia in cells from individuals F1323-21 and NPH309-21 were not significantly different than in control cells (CT1) but longer than in cells from individuals of the BN family. Scale bars represent 5 μm.

PDE6A (c.2053G>A [p.Val685Met]), previously associated with RP[13] (MIM: 180071), that segregated with RP in affected siblings but was not found in individual BN-22 (Figure S5). Altogether, these results show that RP and NPH in the BN siblings are caused by biallelic mutations in two different genes and that mutations in *MAPKBP1* are associated with NPH without RP as observed in individual BN-22. Additional manifestations were observed in several affected individuals from different families including facial dysmorphism (F1323-21 and NPH309-23) and/or scoliosis (NPH309-21, -22, -23). Finally, congenital heart disease and meningomyelocele were observed in a BN family member (BN-23). It remains speculative at this point whether defects of MAPKBP1 are truly related to these conditions since none of them were observed in animal models (see below).

MAP-kinase binding protein 1 (MAPKBP1, also known as JNKBP1) is the paralog of WDR62,[14] the product of a gene mutated in primary microcephaly (*MCPH2* [MIM: 604317]),[15,16] which localizes at the mitotic spindle poles (MSPs) and has been involved in the orientation of the mitotic spindle.[17] MAPKBP1 and WDR62 share the same structural organization with their N-terminal half characterized by the presence of WD40 repeats (12 for MAPKBP1, see Figure 1B). In addition, MAPKBP1,[18] as well as WDR62,[19] binds JNK family members through their C-terminal domain (aa 1,063–1,331 for MAPKBP1). It was shown to act as a scaffolding protein for JNK as well as for other signaling pathways.[18,20,21] Finally, MAPKBP1 and WDR62 also share a highly conserved C-terminal coiled-coil containing region that is required for WDR62 homodimerization and some evidence indicates that it might also be involved in MAPKBP1-WDR62 heterodimerization.[22] However, despite their similarity, no functional relationship has been characterized between the two proteins.

Expression of endogenous MAPKBP1 was tested in vitro and in vivo, using a commercial rabbit polyclonal antibody against MAPKBP1 that we validated by western blot and immunofluorescence experiments (Figures S6A–S6C). Analysis of the expression of MAPKBP1 in fibroblasts from both control subjects and affected individuals using the validated antibody led to the expected results (Figure S6D) with a slightly shorter protein for BN-22 (p.Arg1465*) and no detectable protein for NPH309-21 (p.Gln943*, loss of the epitope) and F1323-21 (p.Arg440*, see Figure S3).

We then investigated the subcellular distribution of MAPKBP1 first in ciliated RPE1 cells. Endogenous (Figure 3A) and V5-tagged MAPKBP1 (Figure 3B) showed

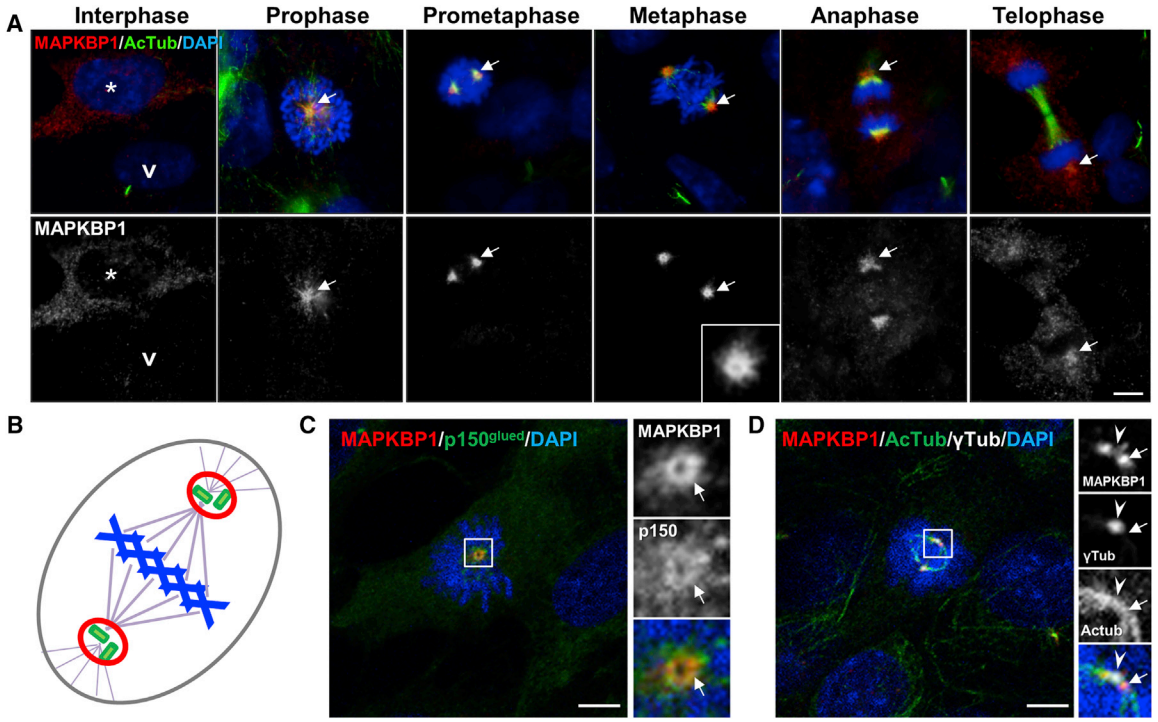

Figure 4. MAPKBP1 Is Recruited to Mitotic Spindle Poles during Early Stages of Mitosis
(A) Cycling RPE1 cells were fixed (PFA) and stained for MAPKBP1 (red) and for DNA with DAPI (blue). Arrows stress accumulation of MAPKBP1 staining at spindle poles in mitotic cells. The white arrowhead and star indicate representative ciliated and non-ciliated cells, respectively. Corresponding MAPKBP1 staining are shown in black and white in the lower panels.
(B) Scheme indicating mitotic spindle poles (MSP, red) surrounding centrosomes (green) at each pole of the mitotic spindle (pink) during metaphase (chromosomes in blue).
(C and D) Cycling RPE1 cells were fixed (PFA) and stained for MAPKBP1 (red) and either with p150 glued (MSP, green [C]; mouse monoclonal antibody [610473, BD Biosciences], dil 1/100) or acetylated α-tubulin (AcTub, spindle, green [D]) and γ-tubulin (γ-tub, centrioles, white [D]; goat polyclonal antibody [sc-7396, Santa Cruz], dil 1/2,000) together with DAPI (blue). Insets on the right show higher magnifications of representative MSP indicated by a white square in the corresponding images. Arrows and arrowheads point to MAPKBP1 staining at the MSP and to γ-tub, respectively. Scale bars represent 5 μm.

a similar diffuse or punctate cytoplasmic distribution and did not show any specific association with either the axoneme (acetylated α-tubulin, arrows) nor the basal body region (arrowhead) of primary cilia, an expected localization for a *NPHP* gene product. Similar results were obtained in ciliated human primary fibroblasts and IMCD3 kidney cells (Figure S7A) as well as in human adult kidney tubular cells in vivo, where MAPKBP1 showed a similar faint cytoplasmic staining not associated with cilia (Figure S8). The absence of MAPKBP1 from cilia and basal body was in agreement with proteomic and recent proximity-dependent biotinylation studies in which MAPKBP1 was not detected either at cilia or at centrosomes/basal bodies.[23–27] Therefore, as expected, mutations in *MAPKBP1* did not show any impact on ciliogenesis since fibroblasts obtained from affected individuals (NPH309-21, F1323-21, BN-22) formed cilia in similar proportion and with similar length as in cells from control individuals (Figures 3C–3E). Cilia with normal shape were also observed at the apical membrane of tubular epithelial cells from individual BN-23 (Figures 2A, panel 4, and S8). In addition, animal models that were generated, including zebrafish morphants (Figure S9) and mutant (Figures S10 and S11) as well as knock-out (Figure S12) mice, did not show any of the classical ciliopathy-associated phenotypes including body axis curvature, situs inversus, or pronephric cysts in the zebrafish, or situs inversus, polydactyly, or renal tubular cysts in the mouse. In agreement, in the zebrafish larvae, *mapkbp1* was not expressed in the pronephros nor in the Kupffer vesicle and was mostly expressed in somites and in the brain (Figure S13), similarly as reported in mice.[18] Altogether, these data show that MAPKBP1 is not directly nor indirectly involved in ciliary functions. Examination of 18-month-old fish, in which *mapkbp1* is expressed at low level in the kidney (Figure S10B), revealed a slight proportion of *mapkbp1* mutant with dilated tubules associated with fibrosis (1/8; Figure S11). This result, although anecdotal, may reflect a potential role for MAPKBP1 in kidney homeostasis in a long term. The lack of obvious kidney phenotype in mice models even in adults (up to 10 months; Figure S12) was already reported in other *Nphp* knockout mice, including *Nphp1*, *Nphp4*, and *Nphp5*,[28–30] respectively mutated in juvenile isolated NPH[1] and SLS-associated NPH.[1,31,32] In the case of *MAPKBP1*, the lack of kidney phenotype in vertebrate models is possibly linked to either residual functional

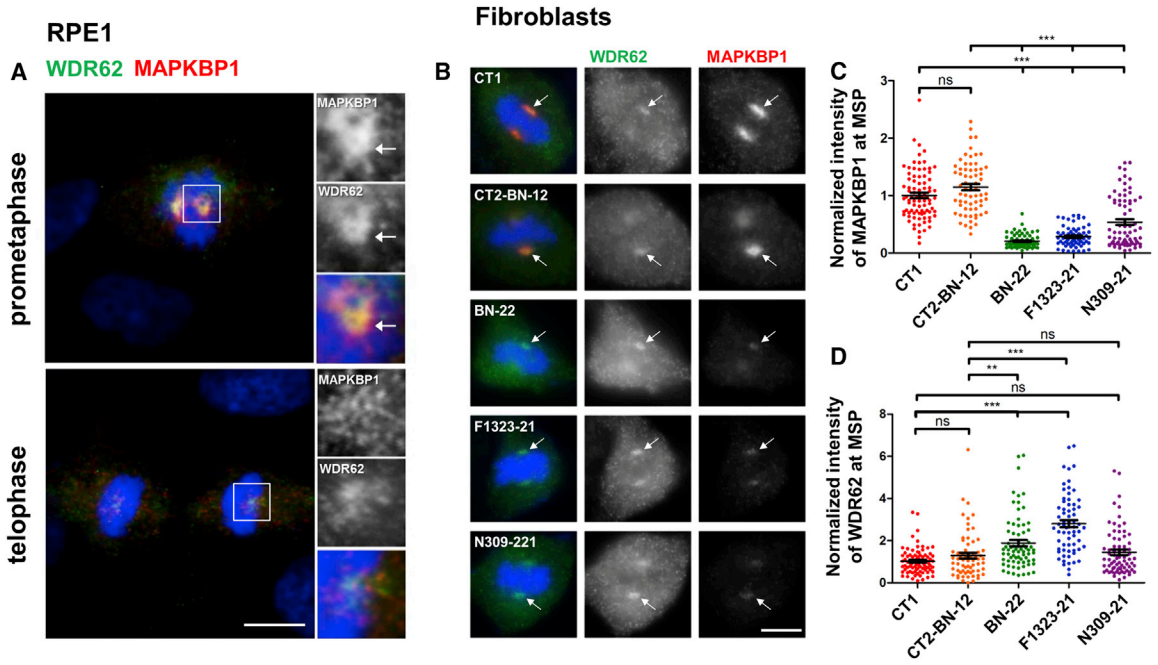

Figure 5. Localization of MAPKBP1 at Mitotic Spindle Poles Is Disturbed in Fibroblasts from Affected Individuals
(A) Cycling RPE1 cells were fixed (PFA) and stained for endogenous MAPKBP1 (red) and WDR62 (green; mouse monoclonal [Clone 3G8, Sigma], dil 1/1,000) together with DAPI (blue). Representative pictures of cells in prometaphase and telophase are shown. Insets on the right show higher magnifications of representative MSP indicated by a white square in the corresponding images.
(B–D) Cycling fibroblasts from control subjects (CT1 and CT2-BN-12) or from affected individuals (BN-22, F1323-21, NPH309-21) were stained for both MAPKBP1 (red) and WDR62 (green). Representative pictures of cells in metaphase are shown in (B). Arrows stress MSPs. Intensity of MAPKBP1 (C) and WDR62 (D) stainings at the mitotic spindle poles was quantified with ImageJ (3 independent experiments, $n > 65$ cells). ns, $^{**}p < 0.001$ and $^{***}p < 0.0001$ were calculated via Dunn's multiple comparison test after the analysis of variance ANOVA test. Scale bars represent 5 μm.

protein (zebrafish mutant) or compensatory effects by its paralog *WDR62* or species- and tissue-specific differences in the function of MAPKBP1.

As MAPKBP1 was absent from cilia in quiescent cells where it showed non-specific cytoplasmic localization (Figures 3 and S7A), we analyzed its distribution in cycling cells. Interestingly, while MAPKBP1 staining was very faint in ciliated quiescent cells, it globally increased in the cytoplasm of non-ciliated cycling cells (Figure 4A, asterisk) and showed a strong accumulation around the poles of the mitotic spindle from prophase to anaphase in mitotic cells (Figure 4A, arrows). Interestingly, this distribution during mitosis was similar to the one reported for WDR62 that is recruited to MSP during early phases of mitosis.[15,17] The localization of MAPKBP1 at MSP was further confirmed by the fact that MAPKBP1 staining showed a typical ring-shaped organization (Figure 4A, metaphase, arrow) that colocalized with the MSP marker p150 glued (Figure 4C, arrows) and it surrounded centrioles as observed by confocal transverse sections (Figure 4D, arrows). MAPKBP1 also colocalized with WDR62 at MSP during early phases of mitosis (Figure 5A), as expected. We therefore investigated the impact of the mutations on the localization of MAPKBP1 and WDR62 during mitosis. As shown in Figure 5B, WDR62 was observed at MSP in mitotic fibroblasts from both control subjects and affected individuals (NPH309-21, F1323-21, BN-22), while MAPKBP1 staining at MSP was severely decreased in affected individuals compared to control subjects (arrows). Quantification of WDR62 and MAPKBP1 staining intensities at MSP confirmed these observations (Figures 5C and 5D). Similar results were obtained upon transient transfections of corresponding V5-tagged MAPKBP1 encoding constructs in cycling HeLa cells (Figure S14), showing that all variants of MAPKBP1, except the p.Arg544Gln, impair its recruitment to MSP. Interestingly, in fibroblasts from two out of three affected individuals (F1323-21 and BN-22, but not NPH309-21), the level of WDR62 staining at MSP was significantly increased compared to control subjects (Figure 5D) suggesting that WDR62 might compensate for the lack of MAPKBP1. In addition, the last conserved coiled-coil domain of MAPKBP1 (aa 1,488–1,514), which is lost in the p.Arg1465* protein (BN-22), was involved in WDR62-MAPKBP1 heterodimerization.[22] As shown in Figures 6A and S15, WDR62 was efficiently co-immunoprecipitated by WT MAPKBP1 but not by the p.Arg1465* variant, confirming the interaction between the two proteins, the role of the last coiled-coil domain in MAPKBP1-WDR62 heterodimerization, and the negative impact of p.Arg1465* on this interaction. As expected, the interaction with WDR62 was also lost for the p.Gln943* shorter protein

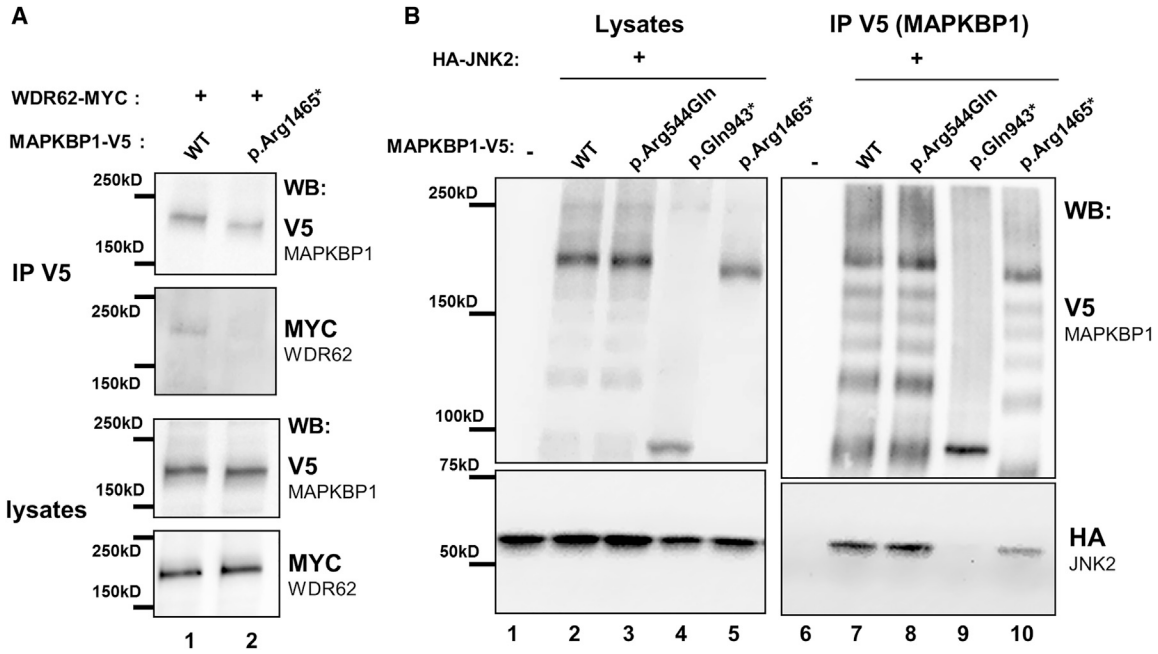

Figure 6. Mutations in *MAPKBP1* Affect JNK2 and/or WDR62 Binding
HEK293 cells were transiently transfected (lipofectamine [ThermoFischer]) with plasmids encoding V5-tagged WT and mutant forms of MAPKBP1 and Myc-tagged WDR62 (A) or HA-tagged JNK2 (B), as indicated. Cells were lysed and immunoprecipitated with the anti-V5 antibody (rabbit polyclonal [Sigma, V8137]). Lysates and immunoprecipitates (IP) were analyzed by western blot as indicated (WB; V5: Mouse monoclonal clone SV5-Pk1 [AbD Serotec MCA-1360], dil 1/5,000; HA: mouse monoclonal, clone 16B12 [Biolegend, 901502], dil 1/5,000; MYC: mouse monoclonal, Ab-2 clone 9E10.3 [Fisher Scientific MS-139-P1], dil 1/5,000).

(NPH309-21). It was preserved for the p.Arg544Gln variant (NPH2139-22; Figure S15), a result in agreement also with the fact that this variation does not affect the WDR62 binding site and with the observation that its targeting to MSP was not affected (Figure S14). Altogether, these data indicate that most of the identified variations in MAPKBP1 affect its recruitment to MSP that is likely to occur through its interaction with WDR62.

The functional impact of the identified mutations was further evaluated by testing their ability to interact with JNK. As shown in Figure 6B, interaction with JNK2 was not affected by the p.Arg544Gln variation (Figure 6B, lane 8; NPH2139-22) as expected by the fact that the N-terminal WD repeat-containing domain is not required for JNK binding.[18,22] Interaction with JNK2 was lost for the p.Gln943* construct (Figure 6B, lane 9; NPH309-21), in agreement with the loss of the reported JNK binding site in this mutant[18] (see Figures 1B and S6A). Moreover, the ability of the p.Arg1465* protein (BN-22) to interact with JNK2 was decreased compared to WT (Figure 6B, lane 10). This could be explained by the fact that the p.Arg1465* variant lacks the last C-terminal coiled-coil that was shown to be involved in dimerization and efficient binding to JNK in the context of WDR62.[22] Despite the effect on JNK binding, *MAPKBP1* mutations did not result in significant change in JNK signaling (phosphorylated JNK) in stable IMCD3 cells knockdown for *Mapkbp1* expression nor in kidney biopsies from affected individual (Figure S16).

Increased DNA damage response (DDR) signaling was recently reported to be associated with NPH-RCs, so we tested whether this was also the case for NPH caused by mutations in *MAPKBP1*. Steady-state DDR signaling was first analyzed in control fibroblasts by immunofluorescence after phosphorylation of H2AX (γH2AX), a widely used marker of DDR signaling.[33] As a positive control for the use of this assay, nuclear γH2AX staining was significantly increased in control fibroblasts treated with aphidicolin, an inhibitor of DNA replication known to induce DDR signaling,[34] compared to untreated cells (Figures S17A and S17B). Steady-state DDR signaling was subsequently analyzed in fibroblasts from affected individuals with mutations in *MAPKBP1*. Interestingly, all mutant fibroblasts showed increased levels of nuclear γH2AX staining compared to healthy controls (Figures 7A and 7B), a phenotype also observed in kidney tubules from affected individual BN-23 (Figure 7C) and in two different murine cell lines (NIH 3T3 and IMCD3) that were knocked-down for Mapkbp1 expression (Figures 7D, 7E, S17E, and S17F). These data are in agreement with those recently reported in other NPH models (*CEP290/NPHP6*, *NEK8/NPHP9*, *SDCCAG8/NPHP10*, *ZNF423/NPHP14*, and *CEP164/NPHP15*)[5,6,8,9,35] and suggest either direct or indirect function of MAPKBP1 in DDR signaling. The exact role of MAPKBP1 in DDR remains to be determined. Interestingly, JNK pathway positively regulates DDR signaling[36] and defects in JNK regulation could then result in the accumulation of non-repaired DNA damage and then in steady-state

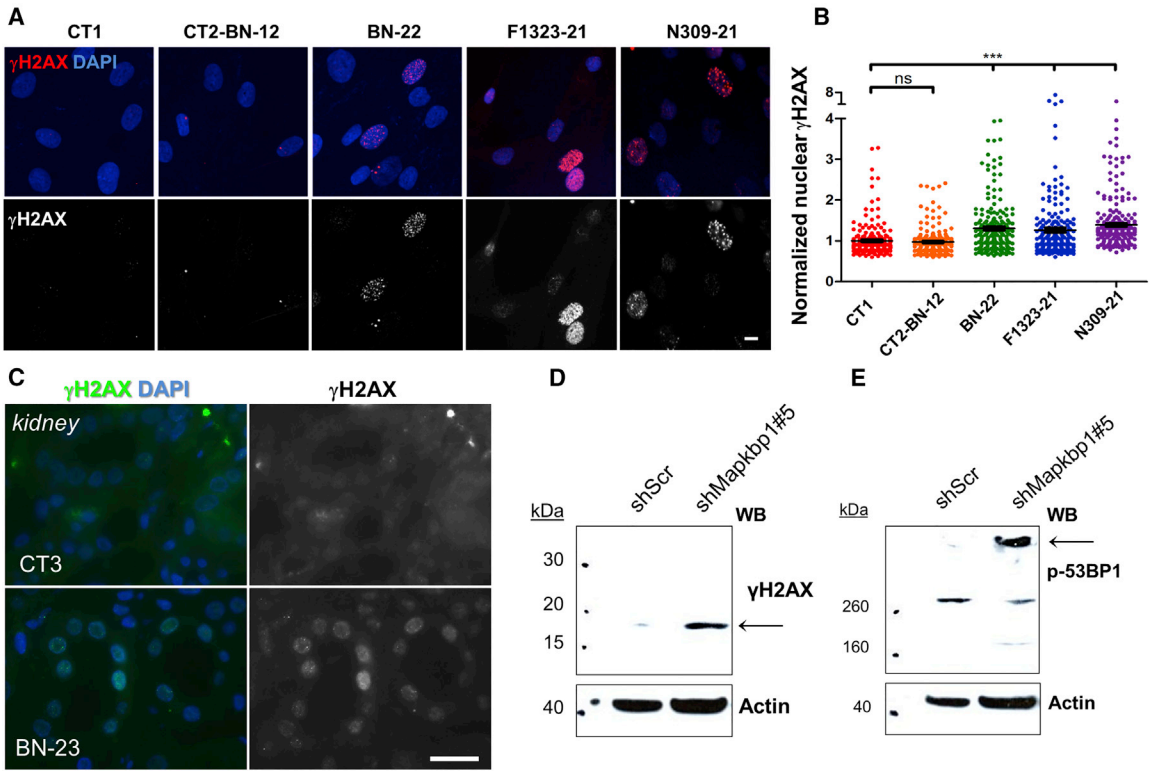

Figure 7. DNA Damage Response Is Increased in MAPKBP1 Mutant Cells

(A) Fibroblasts from control subjects (CT1; CT2-BN-12) and affected individuals (BN-22, F1323-21, NPH309-21) were fixed and stained for phosphorylated γH2AX (red; mouse monoclonal, clone JBW301 [MILLIPORE 05-636], dil 1/200) together with DAPI (blue). Scale bar represents 5 μm.

(B) The intensity of nuclear γH2AX staining was quantified from three independent experiments ($n > 200$). ns and ***$p < 0.0001$ were calculated via Dunn's multiple comparison test after the analysis of variance ANOVA test.

(C) Kidney biopsies from a control unrelated individual (CT3) and from the affected individual BN-23 were stained for γH2AX (green; rabbit polyclonal, dil 1/200). Scale bar represents 20 μm.

(D and E) NIH 3T3 cells (fibroblasts) were stably transduced with lentiviral vectors expressing either control scrambled (shScr) or *Mapkbp1* targeting shRNA (shMapkbp1#5; Figures S16 and S17). Immunoblots show the expression of different components of DNA damage response signaling including γH2AX (Cell Signaling, rabbit polyclonal, dil 1/1,000); (D) and phospho-53BP1 (Cell Signaling, rabbit polyclonal, dil 1/1,000); (E).

increased DDR signaling (γH2AX). However, we could not detect a major general defect in JNK activation in mutant conditions, suggesting that MAPKBP1 might play a specific function in DDR independent of JNK.

In conclusion, the present study revealed biallelic mutations in *MAPKBP1* in eight affected individuals from five unrelated families presenting with juvenile or late-onset NPH (from 12 to >27 years). We therefore propose *NPHP20* (MIM: 617271) as an alias for *MAPKBP1*. Hypomorphic mutations in ciliary *NPHP* genes have been involved in late-onset NPH including *NPHP3*,[37] *WDR19*,[38] *TTC21B*,[39] and *NPHP5*,[40] whereas truncating or loss-of-function mutations of these genes were associated with early-onset NPH or even more severe cystic kidney disease or syndromic forms of ciliopathies[41–43] in agreement with their key functions at cilia. Affected individuals described here did not share additional manifestations classically observed in ciliopathies, in agreement with the fact that MAPKBP1 is not present at cilia and does not seem to be involved in ciliogenesis. Scoliosis and/or facial dysmorphism were found in several but not all of the affected individuals; however, at this point, we cannot correlate mutations in *MAPKBP1* with these manifestations that might be linked to other genetic causes in these consanguineous families. Interestingly, MAPKBP1 does not appear to be involved in cilia function in vitro and none of the generated animal models developed ciliopathy-like phenotypes. It rather seems that *MAPKBP1* is likely the first member of a non-ciliary gene family for NPH that may account for non-syndromic forms of NPH for which causative mutated genes remain largely to be identified.

Accession Numbers

The phenotype presented in this paper has been named *NPHP20* with the MIM accession number 61721.

Supplemental Data

Supplemental Data include 17 figures and 2 tables and can be found with this article online at http://dx.doi.org/10.1016/j.ajhg.2016.12.011.

Acknowledgments

We are grateful to the families and studied individuals for their contribution. We would like to thank Hervé Enslen, Sylvie Legrand-Poels, and Ami Aronheim for their kind gifts of JNK2, MAPKBP1, and WDR62 encoding plasmids; Christelle Arrondel for her precious help for immunohistochemistry; Gérard Pivert (Pathology Department, Necker Hospital) for kidney biopsies; the bioinformatic Plateform (Université Paris Descartes, Institut Imagine) as well as Solenn Pruvost and Mohammed Zarhrate for their support in exome sequencing; Morgan Gallazzini for his kind help on Phospho-JNK blots; Marie-Claire Gubler for her precious help with interpretation of kidney biopsies; Jorunn Skeie Bringsli for genotyping; Torbjørn Leivestad at the Norwegian Renal Registry; and Joseph Szustakowski for his contribution in the early part of the project. The *Mapkbp1* mutant mice were obtained from the Medical Research Council centre for mouse genetics (MRC-Harwell) which distributes these mice on behalf of the European Mouse Mutant Archive. The MRC-Harwell is also a member of the International Mouse Phenotyping Consortium (IMPC), which funded the generation of the *Mapkbp1* mutant mice. This work was supported by grants from the Regional Health Authority Western Norway (grants no. 911688 and 911466 to C.B. and 911746 to E.R.), from the NIH (DK068306 to F.H.), from the Fondation pour la Recherche Médicale (FRM; DEQ20130326532 to S.S.), and the foundation GIS-Maladies Rares (FONDATION_HTS-RD; I201302013 to S.S.). The Imagine Institute is supported by an ANR grant ANR-A0-IAHU-01 and from Fondation ARC (EML20110602384) for the purchase of the LEICA SP8 confocal microscope.

Received: May 13, 2016
Accepted: December 8, 2016
Published: January 12, 2017; corrected online February 2, 2017

Web Resources

Cn3D, http://www.ncbi.nlm.nih.gov/Structure/CN3D/cn3d.shtml
COILS, http://www.ch.embnet.org/software/COILS_form.html
Ensembl Genome Browser, http://www.ensembl.org/index.html
ESEfinder3.0, http://krainer01.cshl.edu/cgi-bin/tools/ESE3/esefinder.cgi?process=home
GenBank, http://www.ncbi.nlm.nih.gov/genbank/
Infrafrontier, https://www.infrafrontier.eu/
International Mouse Phenotyping Consortium, http://www.mousephenotype.org/data/genes/
Jalview, http://www.jalview.org/
MutationTaster, http://www.mutationtaster.org/
NHLBI Exome Sequencing Project (ESP) Exome Variant Server, http://evs.gs.washington.edu/EVS/
OMIM, http://www.omim.org/
PolyPhen-2, http://genetics.bwh.harvard.edu/pph2/
RefSeq, http://www.ncbi.nlm.nih.gov/RefSeq
UCSC Genome Browser, http://genome.ucsc.edu

References

1. Wolf, M.T.F. (2015). Nephronophthisis and related syndromes. Curr. Opin. Pediatr. *27*, 201–211.
2. Bizet, A.A., Becker-Heck, A., Ryan, R., Weber, K., Filhol, E., Krug, P., Halbritter, J., Delous, M., Lasbennes, M.-C., Linghu, B., et al. (2015). Mutations in TRAF3IP1/IFT54 reveal a new role for IFT proteins in microtubule stabilization. Nat. Commun. *6*, 8666.
3. Schueler, M., Braun, D.A., Chandrasekar, G., Gee, H.Y., Klasson, T.D., Halbritter, J., Bieder, A., Porath, J.D., Airik, R., Zhou, W., et al. (2015). DCDC2 mutations cause a renal-hepatic ciliopathy by disrupting Wnt signaling. Am. J. Hum. Genet. *96*, 81–92.
4. Hildebrandt, F., Benzing, T., and Katsanis, N. (2011). Ciliopathies. N. Engl. J. Med. *364*, 1533–1543.
5. Chaki, M., Airik, R., Ghosh, A.K., Giles, R.H., Chen, R., Slaats, G.G., Wang, H., Hurd, T.W., Zhou, W., Cluckey, A., et al. (2012). Exome capture reveals ZNF423 and CEP164 mutations, linking renal ciliopathies to DNA damage response signaling. Cell *150*, 533–548.
6. Slaats, G.G., Saldivar, J.C., Bacal, J., Zeman, M.K., Kile, A.C., Hynes, A.M., Srivastava, S., Nazmutdinova, J., den Ouden, K., Zagers, M.S., et al. (2015). DNA replication stress underlies renal phenotypes in CEP290-associated Joubert syndrome. J. Clin. Invest. *125*, 3657–3666.
7. Otto, E.A., Trapp, M.L., Schultheiss, U.T., Helou, J., Quarmby, L.M., and Hildebrandt, F. (2008). NEK8 mutations affect ciliary and centrosomal localization and may cause nephronophthisis. J. Am. Soc. Nephrol. *19*, 587–592.
8. Grampa, V., Delous, M., Zaidan, M., Odye, G., Thomas, S., Elkhartoufi, N., Filhol, E., Niel, O., Silbermann, F., Lebreton, C., et al. (2016). Novel NEK8 mutations cause severe syndromic renal cystic dysplasia through YAP dysregulation. PLoS Genet. *12*, e1005894.
9. Airik, R., Slaats, G.G., Guo, Z., Weiss, A.-C., Khan, N., Ghosh, A., Hurd, T.W., Bekker-Jensen, S., Schrøder, J.M., Elledge, S.J., et al. (2014). Renal-retinal ciliopathy gene Sdccag8 regulates DNA damage response signaling. J. Am. Soc. Nephrol. *25*, 2573–2583.
10. Slaats, G.G., and Giles, R.H. (2015). Are renal ciliopathies (replication) stressed out? Trends Cell Biol. *25*, 317–319.
11. Failler, M., Gee, H.Y., Krug, P., Joo, K., Halbritter, J., Belkacem, L., Filhol, E., Porath, J.D., Braun, D.A., Schueler, M., et al. (2014). Mutations of CEP83 cause infantile nephronophthisis and intellectual disability. Am. J. Hum. Genet. *94*, 905–914.
12. Cartegni, L., Wang, J., Zhu, Z., Zhang, M.Q., and Krainer, A.R. (2003). ESEfinder: A web resource to identify exonic splicing enhancers. Nucleic Acids Res. *31*, 3568–3571.
13. Corton, M., Blanco, M.J., Torres, M., Sanchez-Salorio, M., Carracedo, A., and Brion, M. (2010). Identification of a novel mutation in the human PDE6A gene in autosomal recessive retinitis pigmentosa: homology with the nmf28/nmf28 mice model. Clin. Genet. *78*, 495–498.
14. Pervaiz, N., and Abbasi, A.A. (2016). Molecular evolution of WDR62, a gene that regulates neocorticogenesis. Meta Gene *9*, 1–9.
15. Nicholas, A.K., Khurshid, M., Désir, J., Carvalho, O.P., Cox, J.J., Thornton, G., Kausar, R., Ansar, M., Ahmad, W., Verloes, A., et al. (2010). WDR62 is associated with the spindle pole and is mutated in human microcephaly. Nat. Genet. *42*, 1010–1014.
16. Yu, T.W., Mochida, G.H., Tischfield, D.J., Sgaier, S.K., Flores-Sarnat, L., Sergi, C.M., Topçu, M., McDonald, M.T., Barry, B.J., Felie, J.M., et al. (2010). Mutations in WDR62, encoding a centrosome-associated protein, cause microcephaly with simplified gyri and abnormal cortical architecture. Nat. Genet. *42*, 1015–1020.

17. Bogoyevitch, M.A., Yeap, Y.Y.C., Qu, Z., Ngoei, K.R., Yip, Y.Y., Zhao, T.T., Heng, J.I., and Ng, D.C.H. (2012). WD40-repeat protein 62 is a JNK-phosphorylated spindle pole protein required for spindle maintenance and timely mitotic progression. J. Cell Sci. *125*, 5096–5109.
18. Koyano, S., Ito, M., Takamatsu, N., Shiba, T., Yamamoto, K., and Yoshioka, K. (1999). A novel Jun N-terminal kinase (JNK)-binding protein that enhances the activation of JNK by MEK kinase 1 and TGF-beta-activated kinase 1. FEBS Lett. *457*, 385–388.
19. Wasserman, T., Katsenelson, K., Daniliuc, S., Hasin, T., Choder, M., and Aronheim, A. (2010). A novel c-Jun N-terminal kinase (JNK)-binding protein WDR62 is recruited to stress granules and mediates a nonclassical JNK activation. Mol. Biol. Cell *21*, 117–130.
20. Yamaguchi, T., Miyashita, C., Koyano, S., Kanda, H., Yoshioka, K., Shiba, T., Takamatsu, N., and Ito, M. (2009). JNK-binding protein 1 regulates NF-kappaB activation through TRAF2 and TAK1. Cell Biol. Int. *33*, 364–368.
21. Lecat, A., Di Valentin, E., Somja, J., Jourdan, S., Fillet, M., Kufer, T.A., Habraken, Y., Sadzot, C., Louis, E., Delvenne, P., et al. (2012). The c-Jun N-terminal kinase (JNK)-binding protein (JNKBP1) acts as a negative regulator of NOD2 protein signaling by inhibiting its oligomerization process. J. Biol. Chem. *287*, 29213–29226.
22. Cohen-Katsenelson, K., Wasserman, T., Darlyuk-Saadon, I., Rabner, A., Glaser, F., and Aronheim, A. (2013). Identification and analysis of a novel dimerization domain shared by various members of c-Jun N-terminal kinase (JNK) scaffold proteins. J. Biol. Chem. *288*, 7294–7304.
23. Andersen, J.S., Wilkinson, C.J., Mayor, T., Mortensen, P., Nigg, E.A., and Mann, M. (2003). Proteomic characterization of the human centrosome by protein correlation profiling. Nature *426*, 570–574.
24. Jakobsen, L., Vanselow, K., Skogs, M., Toyoda, Y., Lundberg, E., Poser, I., Falkenby, L.G., Bennetzen, M., Westendorf, J., Nigg, E.A., et al. (2011). Novel asymmetrically localizing components of human centrosomes identified by complementary proteomics methods. EMBO J. *30*, 1520–1535.
25. Ishikawa, H., Thompson, J., Yates, J.R., 3rd, and Marshall, W.F. (2012). Proteomic analysis of mammalian primary cilia. Curr. Biol. *22*, 414–419.
26. Mick, D.U., Rodrigues, R.B., Leib, R.D., Adams, C.M., Chien, A.S., Gygi, S.P., and Nachury, M.V. (2015). Proteomics of primary cilia by proximity labeling. Dev. Cell *35*, 497–512.
27. Gupta, G.D., Coyaud, É., Gonçalves, J., Mojarad, B.A., Liu, Y., Wu, Q., Gheiratmand, L., Comartin, D., Tkach, J.M., Cheung, S.W.T., et al. (2015). A dynamic protein interaction landscape of the human centrosome-cilium interface. Cell *163*, 1484–1499.
28. Jiang, S.-T., Chiou, Y.-Y., Wang, E., Lin, H.-K., Lee, S.-P., Lu, H.-Y., Wang, C.-K.L., Tang, M.-J., and Li, H. (2008). Targeted disruption of Nphp1 causes male infertility due to defects in the later steps of sperm morphogenesis in mice. Hum. Mol. Genet. *17*, 3368–3379.
29. Won, J., Marín de Evsikova, C., Smith, R.S., Hicks, W.L., Edwards, M.M., Longo-Guess, C., Li, T., Naggert, J.K., and Nishina, P.M. (2011). NPHP4 is necessary for normal photoreceptor ribbon synapse maintenance and outer segment formation, and for sperm development. Hum. Mol. Genet. *20*, 482–496.
30. Ronquillo, C.C., Hanke-Gogokhia, C., Revelo, M.P., Frederick, J.M., Jiang, L., and Baehr, W. (2016). Ciliopathy-associated IQCB1/NPHP5 protein is required for mouse photoreceptor outer segment formation. FASEB J. *30*, 3400–3412.
31. Chaki, M., Hoefele, J., Allen, S.J., Ramaswami, G., Janssen, S., Bergmann, C., Heckenlively, J.R., Otto, E.A., and Hildebrandt, F. (2011). Genotype-phenotype correlation in 440 patients with NPHP-related ciliopathies. Kidney Int. *80*, 1239–1245.
32. Halbritter, J., Porath, J.D., Diaz, K.A., Braun, D.A., Kohl, S., Chaki, M., Allen, S.J., Soliman, N.A., Hildebrandt, F., Otto, E.A.; and GPN Study Group (2013). Identification of 99 novel mutations in a worldwide cohort of 1,056 patients with a nephronophthisis-related ciliopathy. Hum. Genet. *132*, 865–884.
33. Rogakou, E.P., Nieves-Neira, W., Boon, C., Pommier, Y., and Bonner, W.M. (2000). Initiation of DNA fragmentation during apoptosis induces phosphorylation of H2AX histone at serine 139. J. Biol. Chem. *275*, 9390–9395.
34. Ikegami, S., Taguchi, T., Ohashi, M., Oguro, M., Nagano, H., and Mano, Y. (1978). Aphidicolin prevents mitotic cell division by interfering with the activity of DNA polymerase-alpha. Nature *275*, 458–460.
35. Choi, H.J.C., Lin, J.-R., Vannier, J.-B., Slaats, G.G., Kile, A.C., Paulsen, R.D., Manning, D.K., Beier, D.R., Giles, R.H., Boulton, S.J., and Cimprich, K.A. (2013). NEK8 links the ATR-regulated replication stress response and S phase CDK activity to renal ciliopathies. Mol. Cell *51*, 423–439.
36. Shaukat, Z., Liu, D., Hussain, R., Khan, M., and Gregory, S.L. (2016). The role of JNK signalling in responses to oxidative DNA damage. Curr. Drug Targets *17*, 154–163.
37. Olbrich, H., Fliegauf, M., Hoefele, J., Kispert, A., Otto, E., Volz, A., Wolf, M.T., Sasmaz, G., Trauer, U., Reinhardt, R., et al. (2003). Mutations in a novel gene, NPHP3, cause adolescent nephronophthisis, tapeto-retinal degeneration and hepatic fibrosis. Nat. Genet. *34*, 455–459.
38. Bredrup, C., Saunier, S., Oud, M.M., Fiskerstrand, T., Hoischen, A., Brackman, D., Leh, S.M., Midtbø, M., Filhol, E., Bole-Feysot, C., et al. (2011). Ciliopathies with skeletal anomalies and renal insufficiency due to mutations in the IFT-A gene WDR19. Am. J. Hum. Genet. *89*, 634–643.
39. Huynh Cong, E., Bizet, A.A., Boyer, O., Woerner, S., Gribouval, O., Filhol, E., Arrondel, C., Thomas, S., Silbermann, F., Canaud, G., et al. (2014). A homozygous missense mutation in the ciliary gene TTC21B causes familial FSGS. J. Am. Soc. Nephrol. *25*, 2435–2443.
40. Otto, E.A., Loeys, B., Khanna, H., Hellemans, J., Sudbrak, R., Fan, S., Muerb, U., O'Toole, J.F., Helou, J., Attanasio, M., et al. (2005). Nephrocystin-5, a ciliary IQ domain protein, is mutated in Senior-Loken syndrome and interacts with RPGR and calmodulin. Nat. Genet. *37*, 282–288.
41. Tory, K., Rousset-Rouvière, C., Gubler, M.-C., Morinière, V., Pawtowski, A., Becker, C., Guyot, C., Gié, S., Frishberg, Y., Nivet, H., et al. (2009). Mutations of NPHP2 and NPHP3 in infantile nephronophthisis. Kidney Int. *75*, 839–847.
42. Coussa, R.G., Otto, E.A., Gee, H.-Y., Arthurs, P., Ren, H., Lopez, I., Keser, V., Fu, Q., Faingold, R., Khan, A., et al. (2013). WDR19: an ancient, retrograde, intraflagellar ciliary protein is mutated in autosomal recessive retinitis pigmentosa and in Senior-Loken syndrome. Clin. Genet. *84*, 150–159.
43. Davis, E.E., Zhang, Q., Liu, Q., Diplas, B.H., Davey, L.M., Hartley, J., Stoetzel, C., Szymanska, K., Ramaswami, G., Logan, C.V., et al.; NISC Comparative Sequencing Program (2011). TTC21B contributes both causal and modifying alleles across the ciliopathy spectrum. Nat. Genet. *43*, 189–196.

The American Journal of Human Genetics, Volume *100*

Supplemental Data

Mutations in *MAPKBP1* Cause Juvenile or Late-Onset Cilia-Independent Nephronophthisis

Maxence S. Macia, Jan Halbritter, Marion Delous, Cecilie Bredrup, Arthur Gutter, Emilie Filhol, Anne E.C. Mellgren, Sabine Leh, Albane Bizet, Daniela A. Braun, Heon Y. Gee, Flora Silbermann, Charline Henry, Pauline Krug, Christine Bole-Feysot, Patrick Nitschké, Dominique Joly, Philippe Nicoud, André Paget, Heidi Haugland, Damien Brackmann, Nayir Ahmet, Richard Sandford, Nurcan Cengiz, Per M. Knappskog, Helge Boman, Bolan Linghu, Fan Yang, Edward J. Oakeley, Pierre Saint Mézard, Andreas W. Sailer, Stefan Johansson, Eyvind Rødahl, Sophie Saunier, Friedhelm Hildebrandt, and Alexandre Benmerah

Supplemental figures

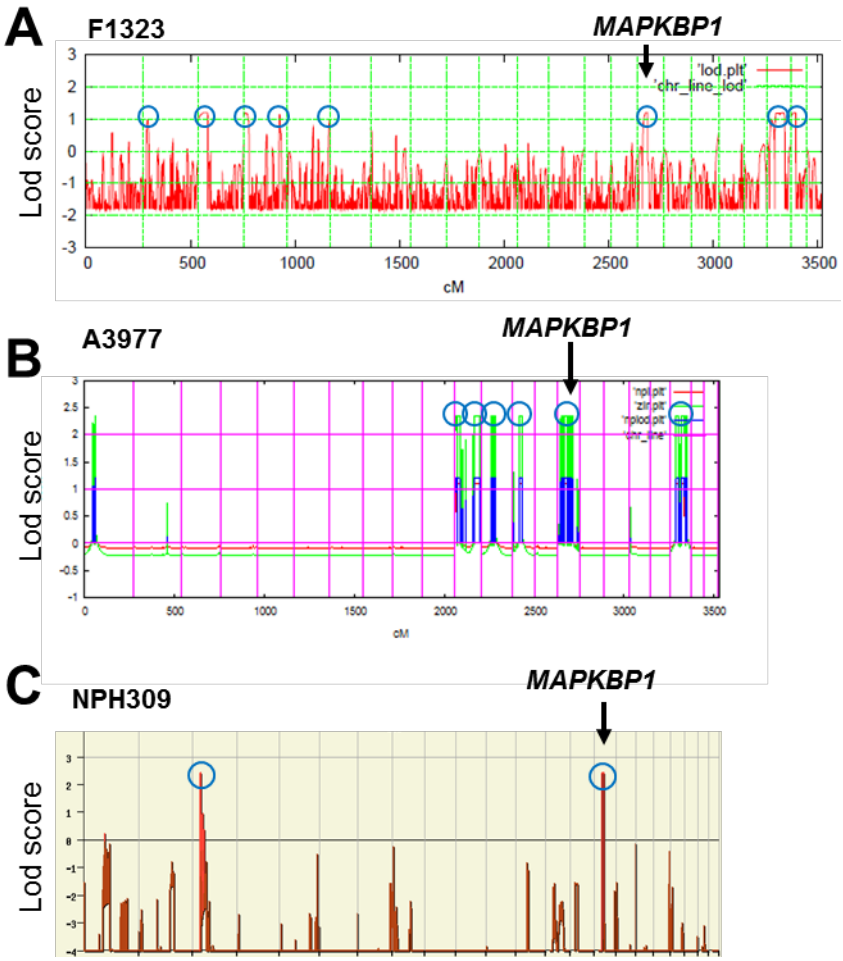

Figure S1: Homozygosity mapping in families F1323, A3977 and NPH309.
For genome-wide homozygosity mapping GeneChip® Human Mapping 250k StyI Array (Affymetrix) was used. Non-parametric LOD scores were identified using MERLIN software for NPH309 and GENEHUNTER 2.1 (PMID: 8651312 / PMID: 10796874) through stepwise use of a sliding window with sets of 110 SNPs and the program ALLEGRO (PMID: 10802644) in order to identify regions of homozygosity, using a disease allele frequency of 0.0001 and Caucasian marker allele frequencies. For graphical presentation nonparametric lod scores (NPL) were calculated and plotted across the human genome. The x axis shows Affymetrix 250K StyI array SNP positions on human chromosomes concatenated from p-ter (left) to q-ter (right). Genetic distance is given in cM. Note that the locus of MAPKBP1 resides within one of the homozygous regions on chromosome 15 (black arrow).

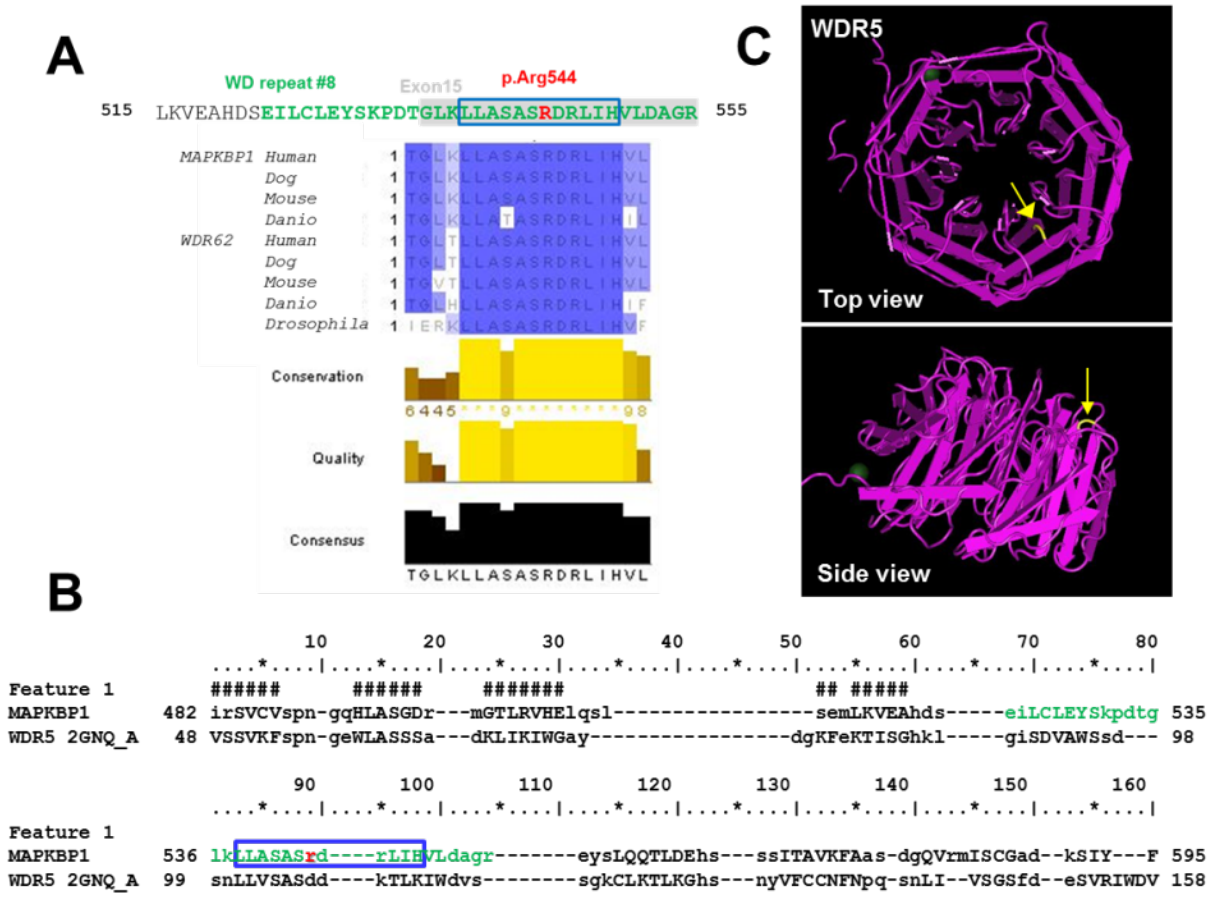

Figure S2: Arg544 is a highly conserved residue likely involved in protein-protein interaction of the WD domain.

A) The Arg544 residue (red) mutated in the NPH2139 family is found in a 12 amino-acid region (boxed in blue) within the eighth WD repeat (green) which is highly conserved among species in both MAPKBP1 and WDR62 as well as in the unique ortholog in *Drosophila*. Sequence alignment was made using Jalview (http://www.jalview.org/). **B)** BLAST and CDD analysis at NCBI revealed that the 8th WD repeat containing the Arg544 residue shows some similarity with one of the WD repeat from the WDR5 protein, which structure has been solved[1]. **C)** Analysis of the 3D structure of the whole WD domain of WDR5 using Cn3D 4.3 (http://www.ncbi.nlm.nih.gov/Structure/CN3D/cn3d.shtml; 2GNQ_A) indicates that the D107 (yellow) corresponding to Arg544 in MAPKBP1 (red) is pointing toward the "top" of the blade and was shown to be required for the interaction of WDR5 with Histone H3[2].

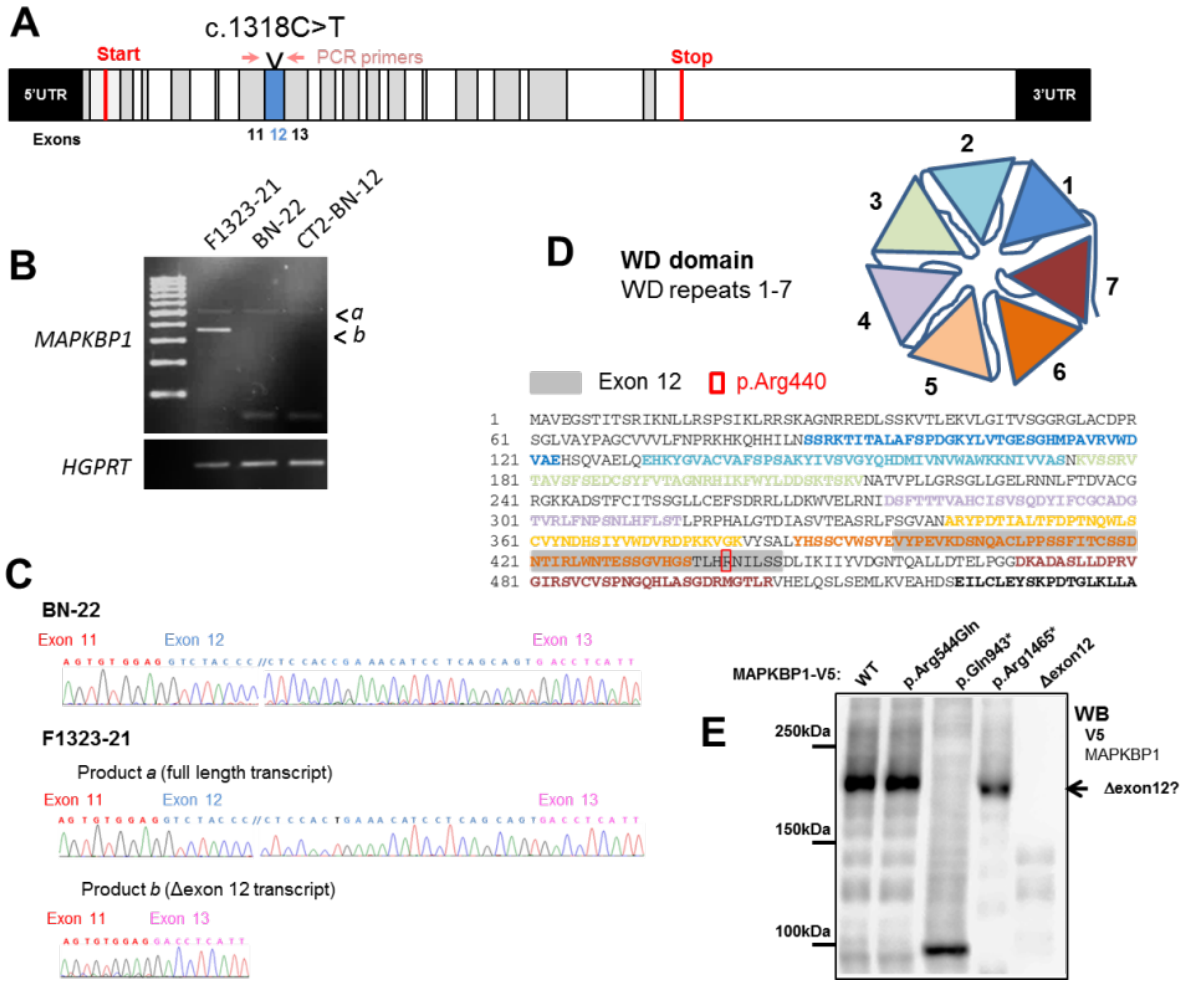

Figure S3: Exon 12 is skipped in F1323-21 individual homozygous for the c.1318C>T mutation.

A) Primers in exons 11 and 13 were designed to amplify exon 12 in which the c.1318C>T mutation is present (MKBP1-primer-11F: 5'-TCTTCTCTGGAGTGGCGAATG-3', MKBP1-primer-13R: 5'-TAAGTGTGCCCATACGGTCCG-3'). **B**) The 11-13 exon region was amplified by RT-PCR from RNA isolated from cycling fibroblasts from F1323-21 and BN-22 affected individuals as well as from control individual CT2-BN-12 (mother of BN-22; see Fig.1). Two PCR products were amplified from the F1323-21 individual samples, one of the expected size also found in the other individuals (product a) and one smaller fragment only found in this affected individual (product b). **C**) RT-PCR products from BN-22 and F1323-21 individuals were sequenced by Sanger and corresponding chromatograms are shown with the mutated nucleotide indicated in black. **D**) Scheme showing the organization of a typical WD domain which is composed of 7 WD repeats and sequence of the N-terminal WD domain of MAPKBP1 where each of the first 7 WD repeats is in the same color as in the scheme. The p.Arg544 residue is boxed in red and exon 12 encoded region in grey. **E**) Lysates of HEK293 cells transiently transfected with the indicated V5-tagged MAPKBP1 encoding plasmids were analyzed by western-blot (WB) using the rabbit polyclonal antibody against the V5 epitope (see **Figure S6**). Expected size of the Δexon12 is indicated by an arrow.

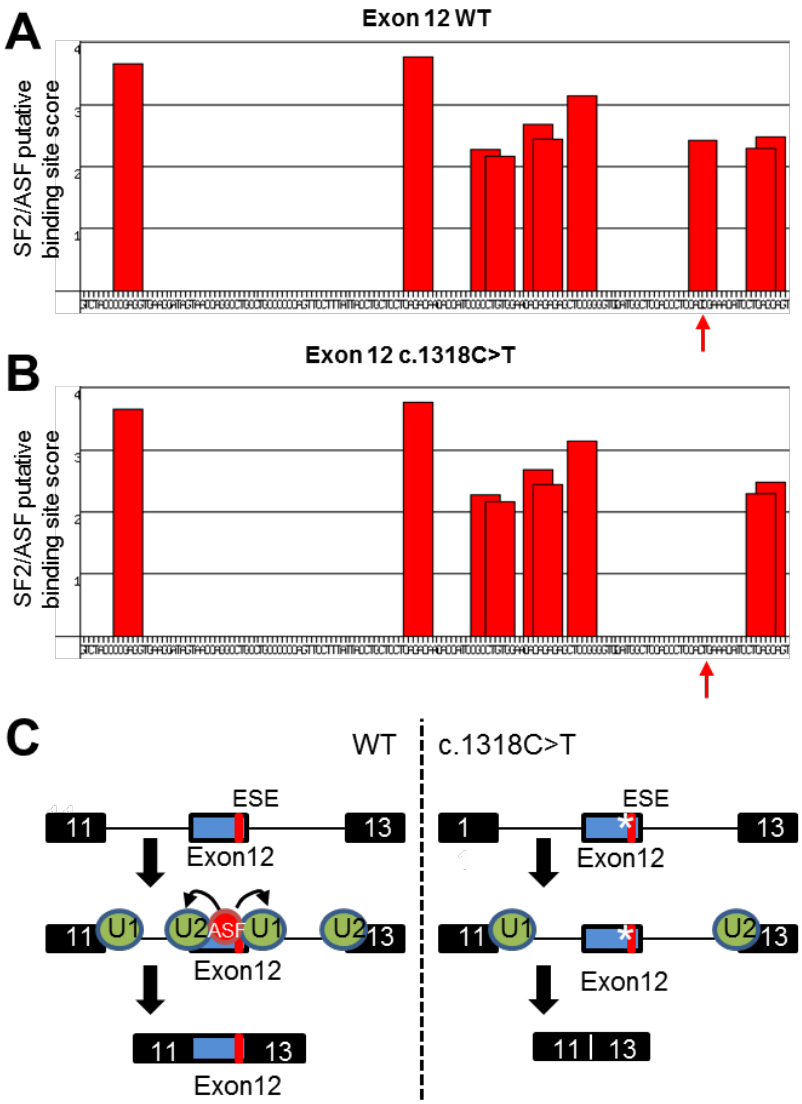

Figure S4: The c.1318C>T mutation in exon 12 is predicted to affect a SR protein binding site.

A-C) Sequence of WT (**A**) and mutated (**B**) exon 12 were subjected to ESEfinder (http://krainer01.cshl.edu/cgi-bin/tools/ESE3/esefinder.cgi?process=home)[3] to check for putative binding of serine-arginine rich (SR) proteins on exonic splicing enhancer (ESE) which then bind to splicing factors (U; **C**). ESEfinder analysis revealed that the c.1318C>T mutation affects one putative binding site for SF2/ASF and is therefore likely to increase the probability of skipping of exon 12 (red arrow).

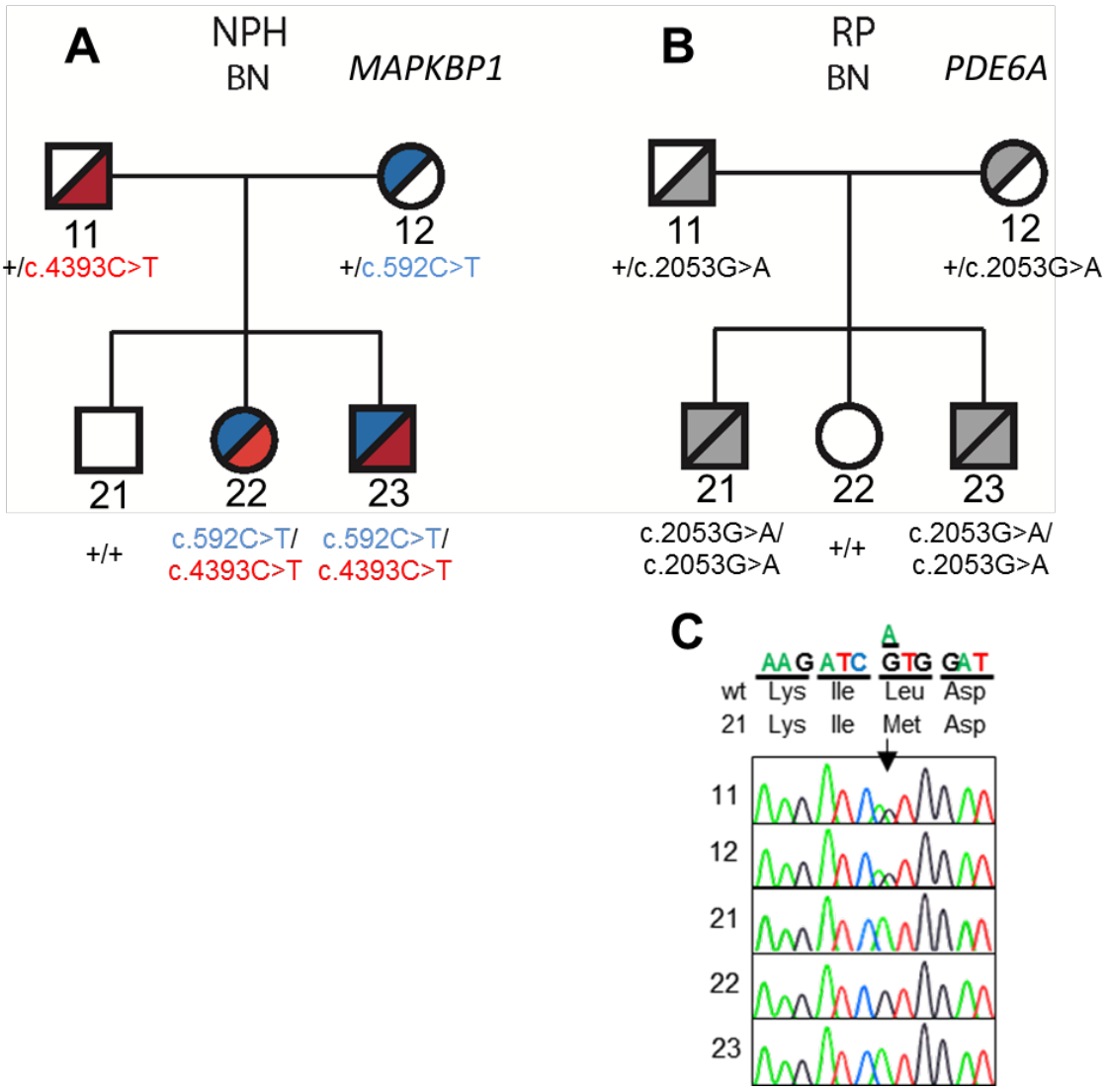

Figure S5: Segregation of nephronophthisis and retinitis pigmentosa in the BN family.

A-B) The affected individuals BN-22 and BN-23 were compound heterozygous for mutations in *MAPKBP1* (c.592C>T (blue) and c.4393C>T (red); **A**) while BN-21 and BN-23 were homozygous for a mutation in *PDE6A* (c.2053G>A; **B**). **C)** Segregation of the *PDE6A* mutation was analyzed by Sanger sequencing. Segregation of *MAPKBP1* mutations is shown in Fig.1.

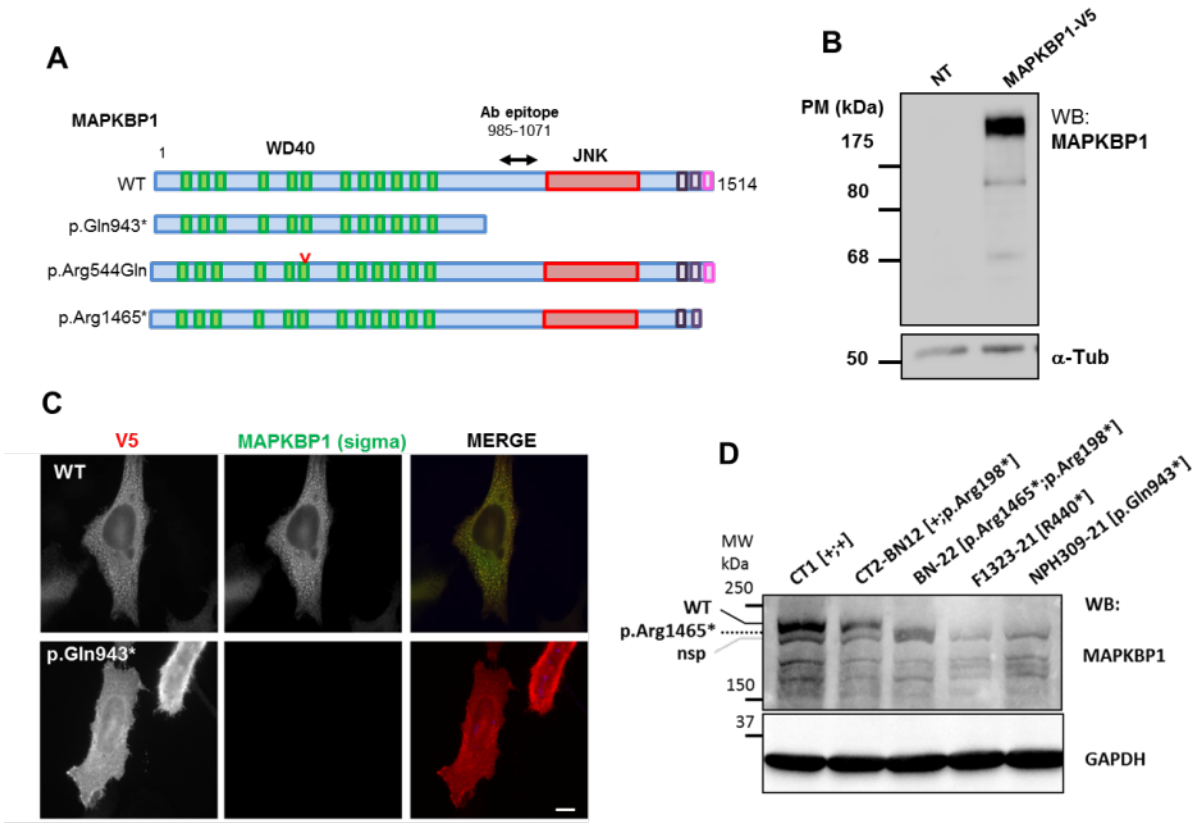

Figure S6: Specificity of the MAPKBP1 antibody.

A) Schema points out the used MAPKBP1 constructs (WT and p.Gln943*) and to the epitope recognized by the Sigma antibody. **B**) Lysates of HEK293 cells transiently transfected or not with the V5-tagged MAPKBP1 encoding plasmid were analyzed by western-blot using a rabbit polyclonal antibody against MAPKBP1 from Sigma (HPA030832; dilution 1/5000) and a mouse monoclonal against alpha-tubulin (clone B-5-1-2, sigma, 1/10.000) as indicated. **C**) HeLa cells transiently transfected with plasmids encoding for V5-tagged WT or p.Gln943* were fixed and stained for V5 (green; mouse monoclonal, clone SV5-Pk1 [AbD Serotec MCA-1360]; dil 1/10.000) and with the MAPKBP1 antibody from Sigma (red). Scale bar: 5 μm. **D**) Lysates of fibroblasts from control (CT1 (healthy unrelated individual), CT2-BN-12) and affected individuals (BN-22, F1323-21, NPH309-21) were analyzed by western-blot using the rabbit polyclonal antibody against MAPKBP1 (HPA030832; dilution 1/1000) and a mouse monoclonal against GAPDH (clone 6C5, Millipore, dil 1/10.000), as indicated. Relative position of full length WT and p.Arg1465* truncated proteins are indicated by black and dotted lanes, respectively. The presence of a nonspecific (nsp) band which migrates just below WT and p.Arg1465* proteins is indicated by a grey lane.

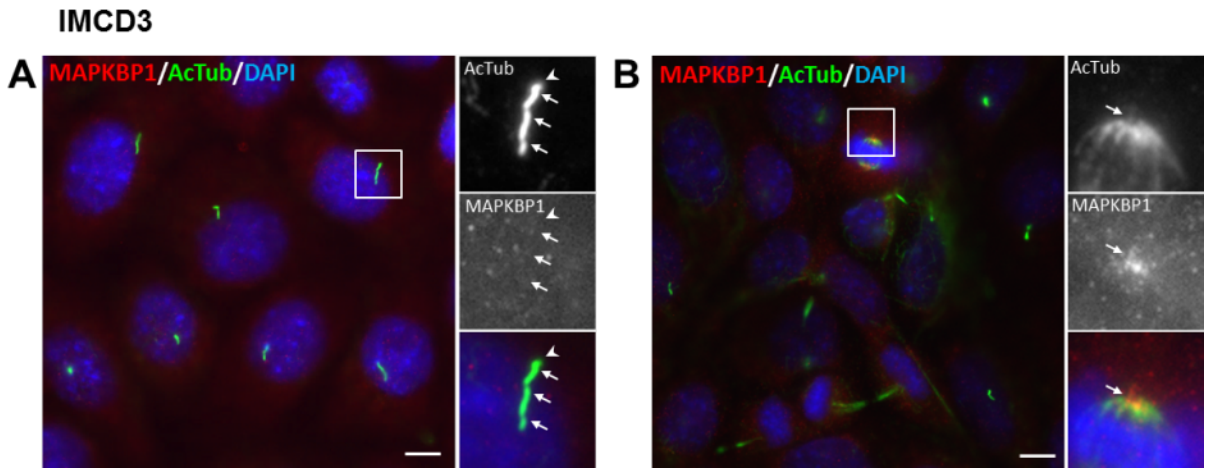

Figure S7: Distribution of MAPKBP1 in ciliated and cycling IMCD3 cells.

Confluent IMCD3 cells were fixed in PFA and stained for acetylated α-tubulin (AcTub, green) and MAPKBP1 (red) similarly as in Figs. 3 and 4. Insets on the right show higher magnifications of representative cilium (**A**) or mitotic spindle pole (**B**) indicated by a white square in the corresponding images. **A**) Arrows indicate cilia, arrowhead cilium base region. **B**) Arrows indicate mitotic spindle pole. Scale bars: 5 μm.

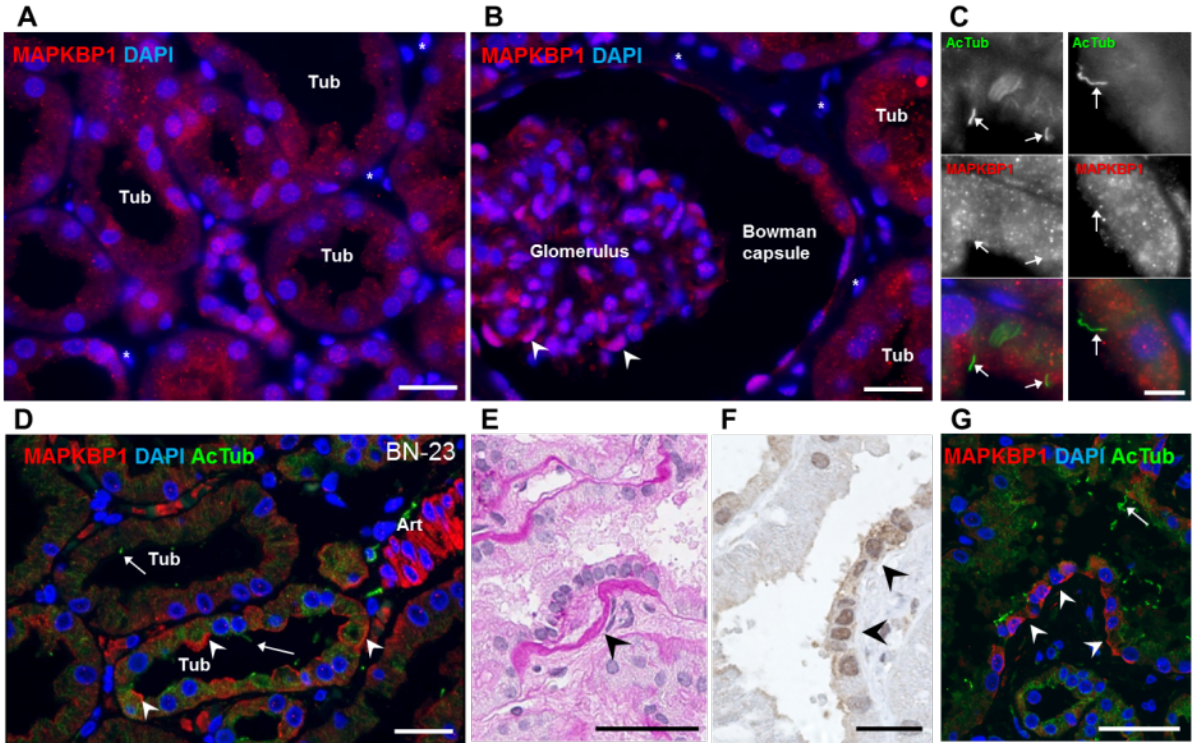

Figure S8: MAPKBP1 shows a diffuse expression pattern in human adult kidney.

A-C) Kidney biopsy from a control individual was stained for MAPKBP1 (red (**A-C**); HPA030832; dil 1/100)) and acetylated tubulin to label cilia (AcTub, green, (**C**); 6–11-B-1, dil 1/500). MAPKBP1 shows a diffuse granular distribution in the cytoplasm of tubular epithelial cells (Tub) as well as in epithelial cells from the Bowman capsule whereas it does not seem to be expressed in interstitial cells (stars). MAPKBP1 is also expressed in cells in glomeruli where it is also found in the nucleus in some cells (arrowheads). MAPKBP1 was not detected in cilia (Arrows). **D)** MAPKBP1 staining (red) in the kidney biopsy of the BN-23 individual. **D** shows tubules (Tub) with focal accentuated staining of tubular epithelial cells and pronounced staining of the smooth musculature of an arteriole (Art). **E-G**) Pictures show a part of proximal tubules with abrupt transition from normal to disorganized basement membrane (**E**, PAS) and to dedifferentiated tubular epithelial cells (arrowheads). This finding is typical but not specific for nephronophthisis. Dedifferentiated tubular epithelial cells express increased positivity for MAPKBP1 (**E**, brown, immunohistochemistry; **G**, red; immunofluorescence). Some cilia are present (**D**, **F**, arrows; AcTub). Scale bars: 20 μm (**A, B, D, F, G**), 50 μm (**E**), 5 μm (**C**).

Figure S9: Injection of *mapkbp1* morpholino does not result in ciliopathy like phenotype.

A-C) Zebrafish embryos were injected with two different *mapkbp1* morpholinos, e2i2 (5'-ATTGAAGTTGAGTTACTCACCCGGC-3') and e4i4 (5'-TTGAGGAATTGAGCACCCACCTCGC-3') targeting exon2:intron2 and exon4:intron4 junctions, respectively. **A)** Efficiency of the used morpholinos on splicing was tested by RT-PCR using primers designed to amplify regions between exon 1 and 3 (e2i2: fw 5'-AGTAAAGCTGGCAACAACAAAGAG-3'/rev 5'-TGCTGTTTGTTCTTCTTAGGGTTC-3') and exons 3 and 5 (e4i4: fw 5'-GAACCCTAAGAAGAACAAACAGCA -3'/rev 5'-CGCCGTATTTATGTTCCTGTAACT-3'). **B)** A representative picture of e2i2 morpholino-injected embryos is shown. **C)** Body axis deformation including curved or deformed) of control and embryos injected with e2i2 or e4i4 morpholinos (1.5mM) was quantified compared to control morpholino-injected embryos (ct). One representative experiment out of two is shown. A morpholino targeting *traf3ip1* (1.5mM) was used in parallel as a positive control and, as expected[4], 85.6% and 83.3% of the injected embryos showed curved body axis and pronephric cysts (not shown), respectively. Experiments on the zebrafish were approved by the "Services Vétérinaires de la Préfecture de Police de Paris" and by the ethical committee of the Paris Descartes University.

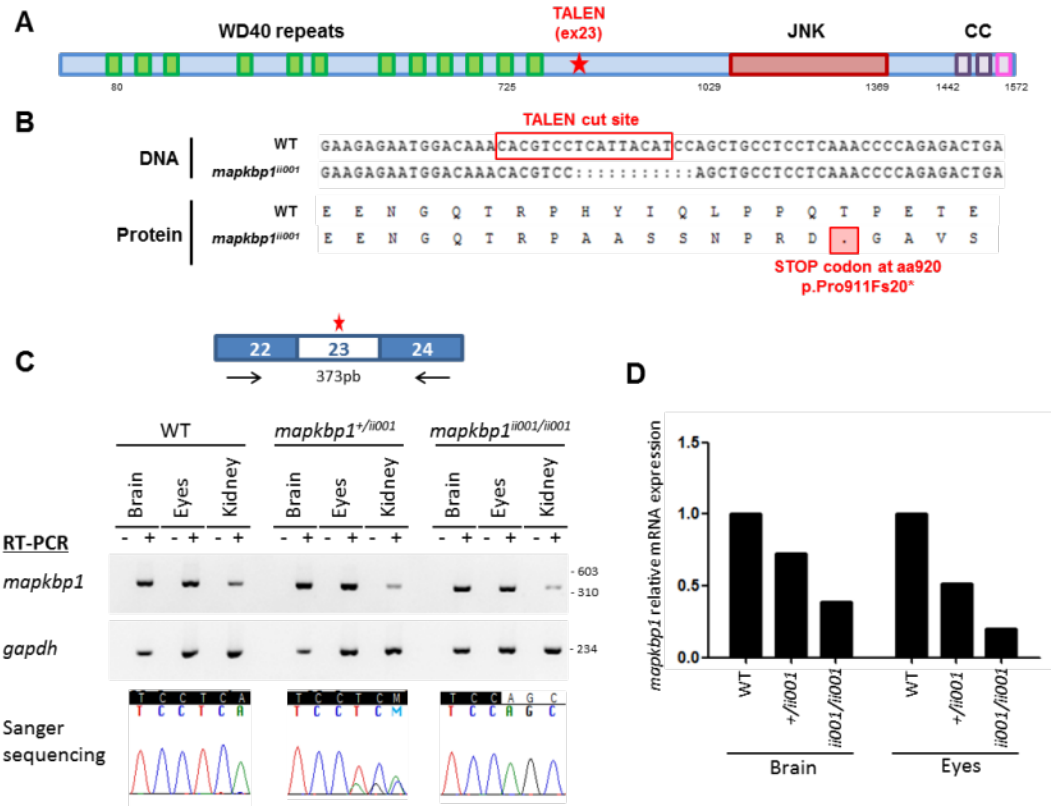

Figure S10: Generation of a *mapkbp1* mutant zebrafish line

A) Schema of Mapkbp1 protein depicting the different functional domains that have been described in the human protein (WD repeats, domain of interaction with JNK, coiled-domain involved in dimerization with WDR62). The TALEN target site in exon 23 is represented in red (star). **B**) DNA and protein sequences of TALEN target site in wild-type and mutated animals. One allele has been identified in F1 generation that deletes 11 base pairs (bp), leading to a frameshift and premature stop codon at amino acid (aa) 920 of zebrafish Mapkbp1 protein. This allele is hereafter referred to as *mapkbp1*^{ii001}. **C**) A 373bp region flanking exon 23 of *mapkbp1* transcript was amplified by RT-PCR from the indicated tissues isolated from WT, heterozygous and homozygous mutant adult (7-month old) fish using primers in exons 22 and 24 (mapkbp1-RTex22_F 5'-TCCATGTTGGACCTGAGACA-3'; mapkbp1-RTex24_R 5'-ACAGGCGACTGCTGGAATAC-3'). *gapdh* was amplified as a positive control (gapdh_F 5'-GTTGGTATTAACGGATTCGGTC-3'; gapdh_R 5'-CACTTAATGTTGGCTGGGTC-3'). Chromatograms from Sanger sequencing of of the TALEN cut site (black) of RT-PCR products from WT, heterozygous and homozygous mutant fishes are shown at the bottom. These data indicate that there is no exon skipping of exon 23 and that the mutation is expressed. **D)** qRT-PCR (SybR Green PCR Master mix, Applied Biosystems) analysis of *mapkbp1* relative expression in WT, heterozygous and homozygous mutant fish show a 80 % (Eyes) and 60% (Brain) decrease compare to WT tissues, indicating RNA decay. *mapkbp1* expression was normalized to *ef1α* expression (mapkbp1-qPCR_F 5'- GGGCTGCTCTGTGAGTTCAA-3'; mapkbp1-qPCR_R 5'- GTGGCCATACTGGTTGCGA-3'; ef1α-qPCR_F 5'- CTGGAGGCCAGCTCAAACAT-3'; ef1α-qPCR_R 5'- ATCAAGAAGAGTAGTACCGCTAGCAT-3'). Of note, expression of *mapkbp1* in kidney tissues was not detectable by qPCR.

Figure S7

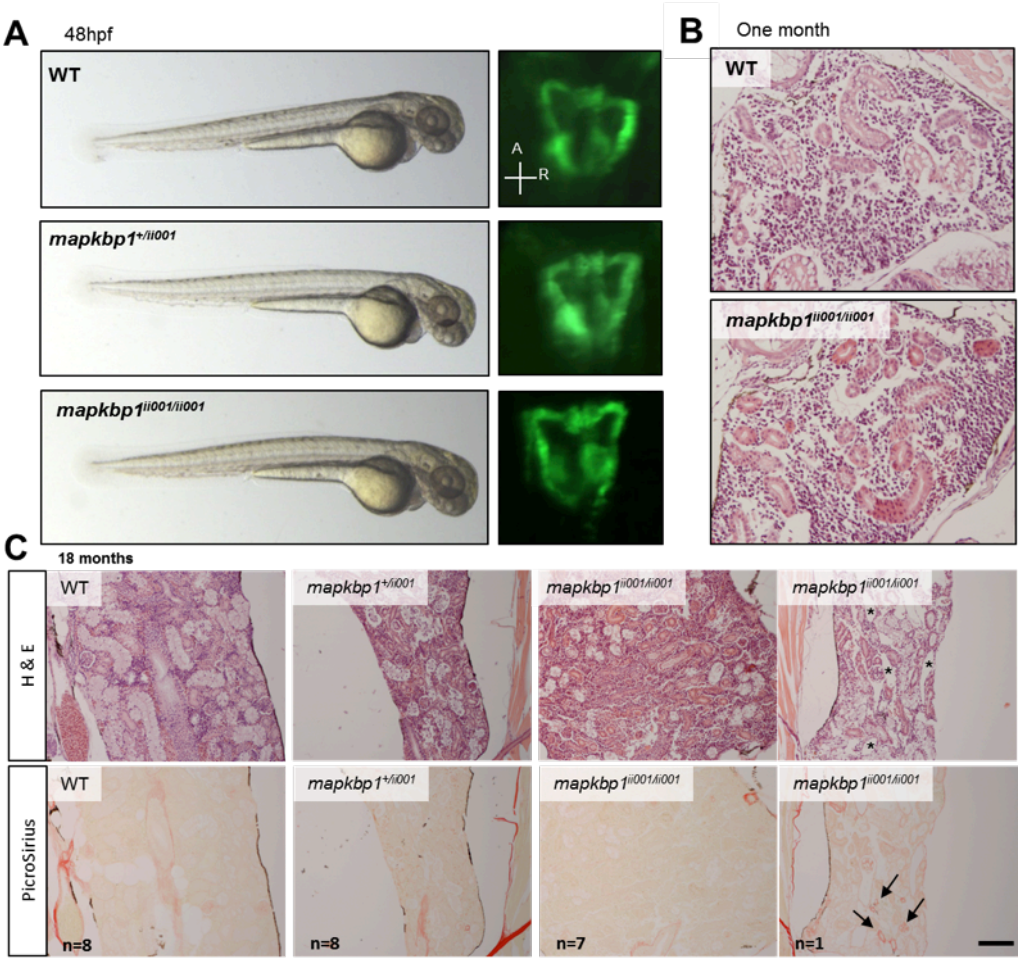

Figure S11: *mapkbp1*$^{ii001/ii001}$ mutant zebrafish embryos do not present ciliopathy-related phenotype

A) *mapkbp1*$^{ii001/ii001}$ mutant animals do not show any obvious phenotype at embryonic (here shown at 48hpf) and larval stages. *Tg(wt1b:GFP)* transgenic embryos allow the visualization of proximal pronephros, that look normal in mutant embryos (dorsal views, anterior (A) to the top). Mutant animals survive till adulthood and are fertile. Maternal-zygotic mutant embryos do not have obvious phenotype either. **B-C**) Histological analysis (H&E) of one-month (B) and 18-month (C) old WT, heterozygous and *mapkbp1*$^{ii001/ii001}$ kidneys revealed no noticeable abnormalities, except in one of the eight aged mutant animals which exhibited tubular dilations (*) associated with slight fibrosis as shown by PicroSirius staining (**C**, right panel; arrows). Scale bar, 200µm.

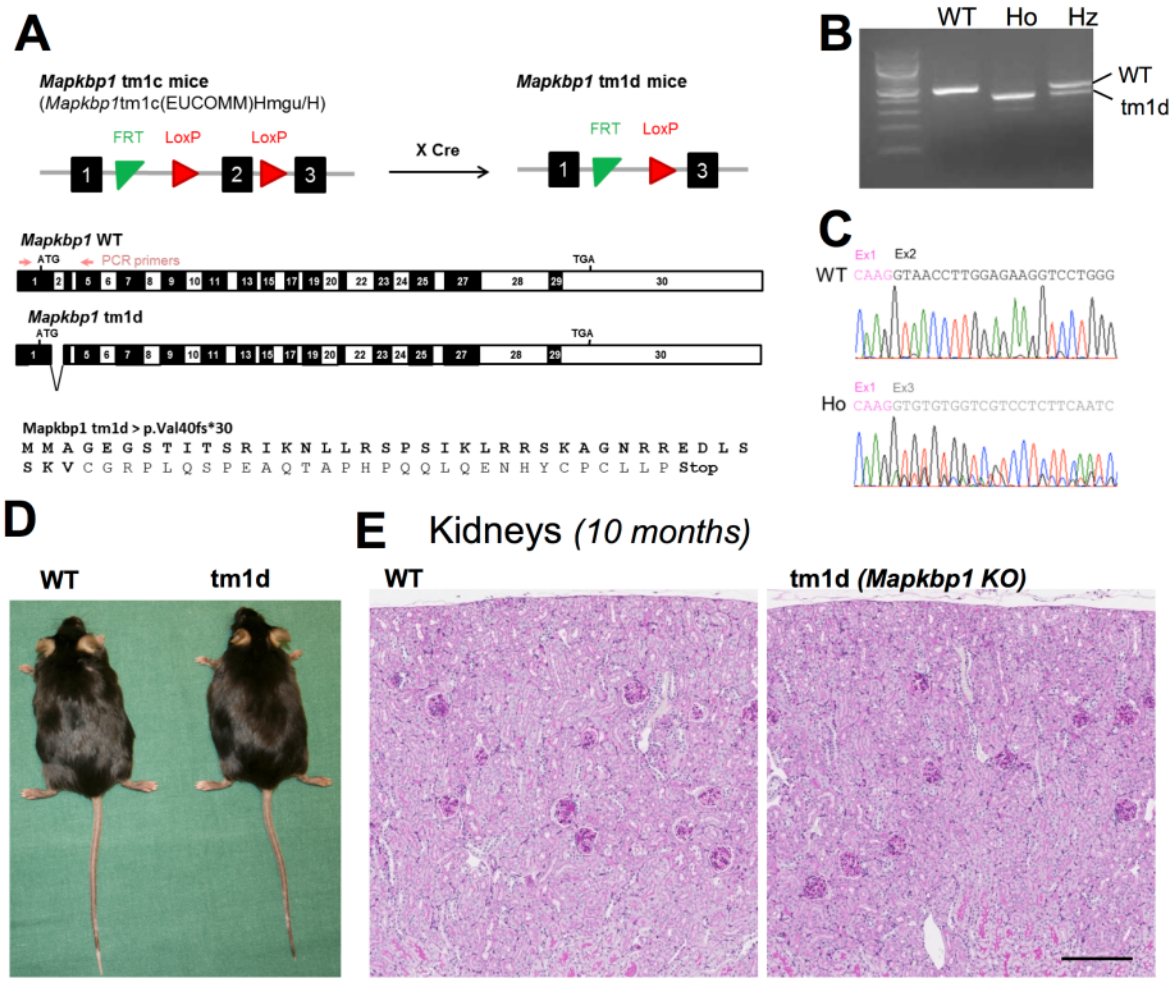

Figure S12: mRNA expression and morphology of kidneys from *tm1d Mapkbp1* mice.

A) *Mapkbp1* tm1c mice (*Mapkbp1*tm1c(EUCOMM)Hmgu/H) and Cre-expressing mice (C57BL/6NTac-Tg(ACTB-cre)3Mrt/H) were obtained from MRC-Harwell (UK) and bred to generate *Mapkbp1* tm1d mice. In the tm1c mice, exon 2 of *Mapkbp1* is flanked by two LoxP sites (http://www.mousephenotype.org/data/alleles/MGI:1347004/tm1c(EUCOMM)Hmgu/) which was then exised by the Cre recombinase. Exon2 is 92 nucleotides long, it is not in frame and its deletion is predicted to lead to frame shift with introduction of a stop codon 30 aminoacids after p.Val40. **B**) RT-PCR analysis of *Mapkbp1* expression. RNA was extracted from kidneys of wild-type (WT), heterozygous (Hz) or homozygous (Ho) mice and the exon1-exon5 region was amplified by RT-PCR (MAPKBP1-mus-cds-1-1F 5'-catatccgaaggctgtgttg-3', MAPKBP1-mus-cds-1-1R 5'-tagctctgccacctggctac-3'). The cDNA from the mouse homozygous for the *Mapkbp1* tm1d allele has a shorter transcript compared to WT corresponding to the lack of exon 2. **C**) Chromatograms from Sanger sequencing of PCR products from homozygous and WT mice obtained as in **B**. Sequences corresponding to exon 1 are indicated in pink whereas exon 2 and exon 3 are indicated in black and grey respectively. **D**) Pictures of representative WT and tm1d Mapkbp1 KO mice. **E**) Histologic examination (PAS staining) of kidneys of wild-type (WT) and homozygous (*Mapkbp1* KO) 10 months of age mice shows no pathology. Scale bar: 200 μm. Works on mice were approved by the Norwegian Food Safety Authority (FOTS 8367).

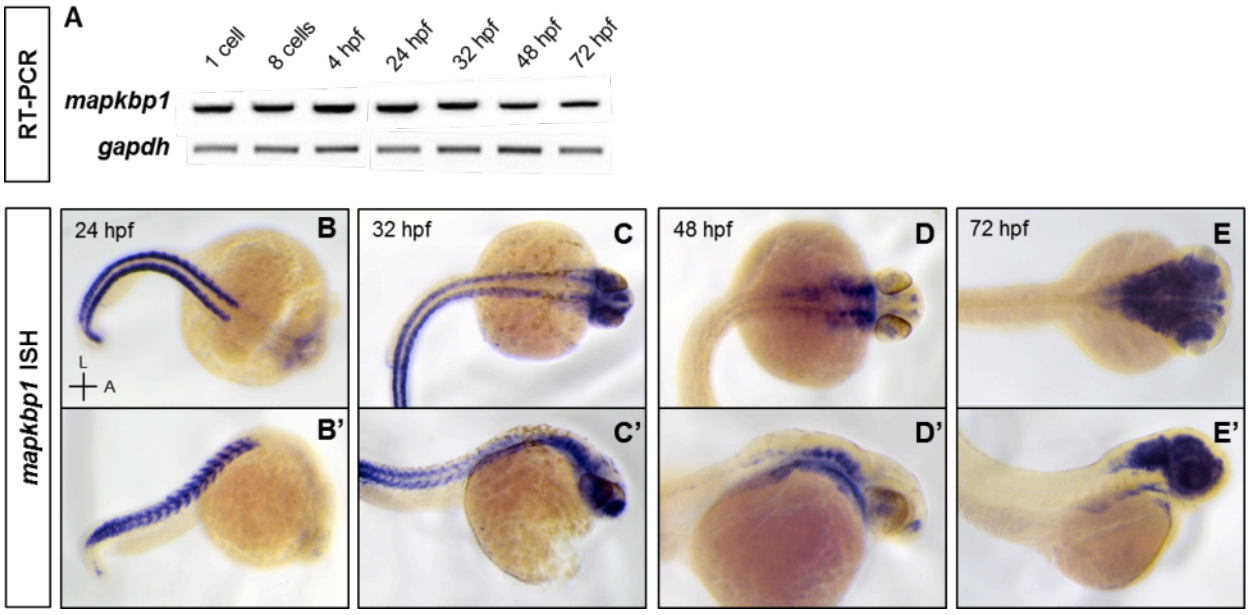

Figure S13: Expression pattern of *mapkbp1* during zebrafish early development

A) RT-PCR analysis of *mapkbp1* expression performed on WT zebrafish embryos. Expression at 1-cell and 8-cell stages indicate a maternal contribution of *mapkbp1* transcripts. **B-E**) Whole mount *in situ* hybridization of *mapkbp1* at 24, 32, 48 and 72 hours post fertilization (hpf). At 24 hpf, a strong expression is observed in the somites and then in the head at 32 hpf. From 48 hpf, *mapkbp1* expression starts to be restricted to the brain. Noteworthy, no expression is detected in the pronephros during embryonic developmental stages. Dorsal (top, **B-E**) and lateral (bottom, **B'-E'**) views, anterior to the right.

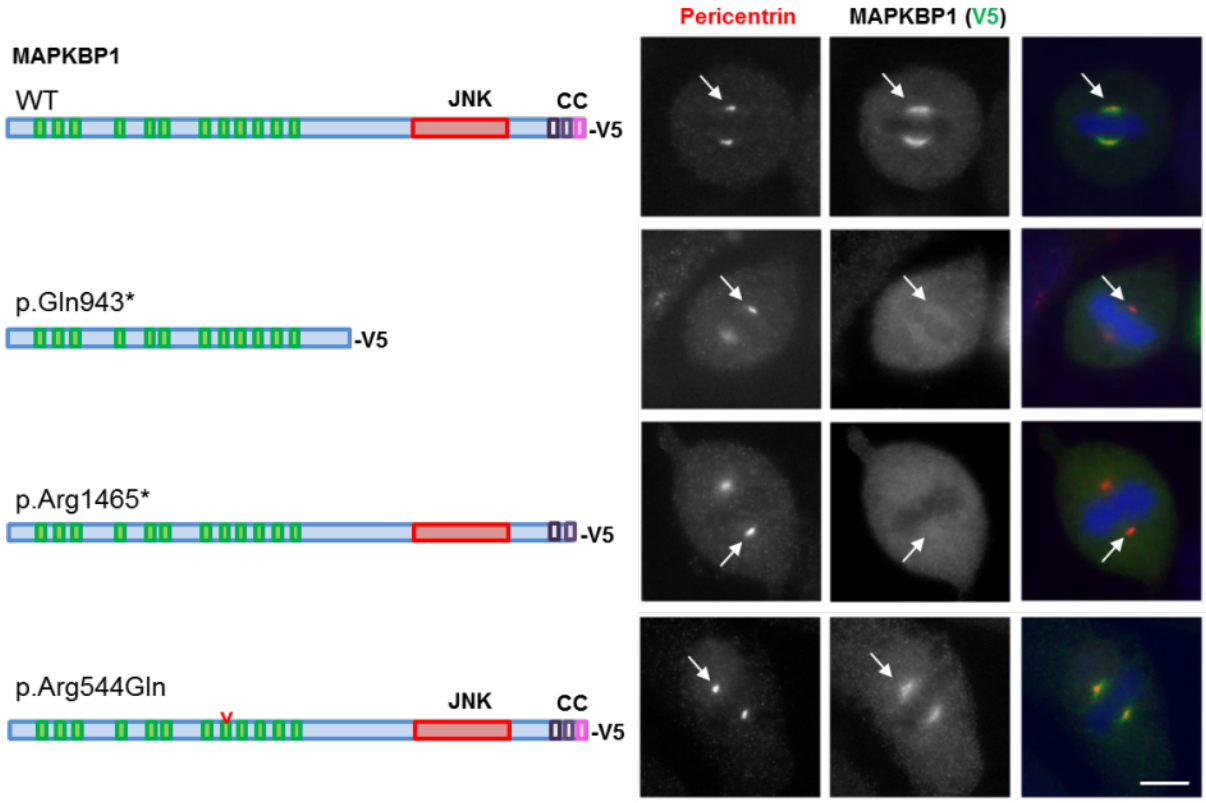

Figure S14: Impact of mutations on the targeting of MAPKBP1 to mitotic spindle poles.
HeLa cells transiently transfected with indicated MAPKBP1 WT and mutant V5-tagged constructs were fixed in PFA (4%) and stained for pericentrin (red; rabbit polyclonal, Abcam ab4448, dil 1/3.000) and V5 epitope (MAPKBP1, green; mouse monoclonal, clone SV5-Pk1, AbD Serotec MCA-1360, dil 1/10.000).

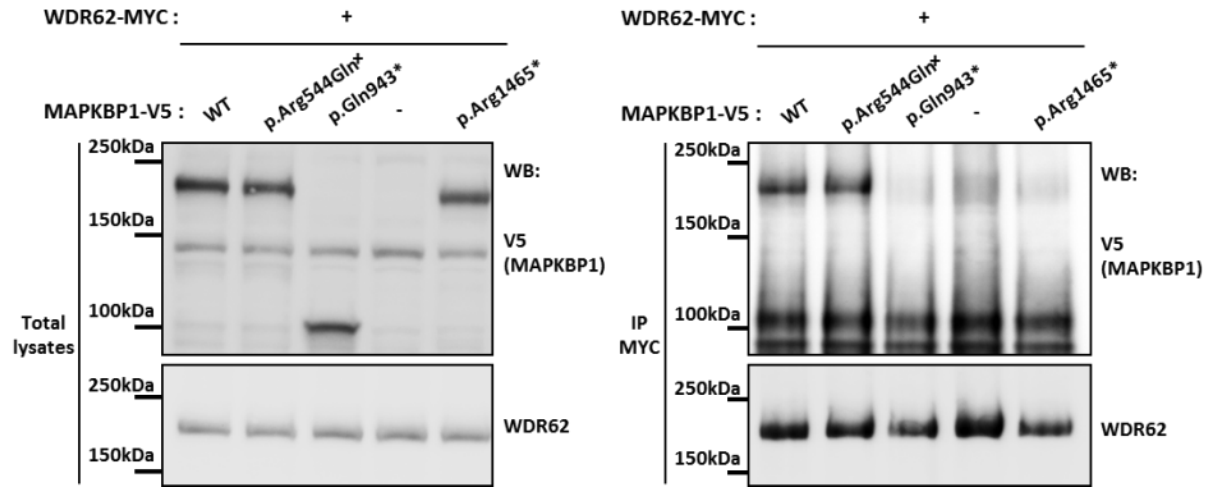

Fig.S15: Impact of *MAPKBP1* mutations on the interaction with WDR62.

HEK293 cells were transiently transfected (lipofectamine [ThermoFischer]) with plasmids encoding V5-tagged WT and mutant forms of MAPKBP1 and Myc-tagged WDR62, as indicated. Cells were lyzed and immunoprecipitated with the anti-myc antibody (MYC: mouse monoclonal, Ab-2 clone 9E10.3 [Fisher Scientific MS-139-P1]). Lysates and immunoprecipitates (IP) were analyzed by western-blot as indicated (WB; V5: Mouse monoclonal clone SV5-Pk1 [AbD Serotec MCA-1360], dil 1/5000; WDR62: rabbit polyclonal [NB100-77302, NOVUS], dil 1/5000).

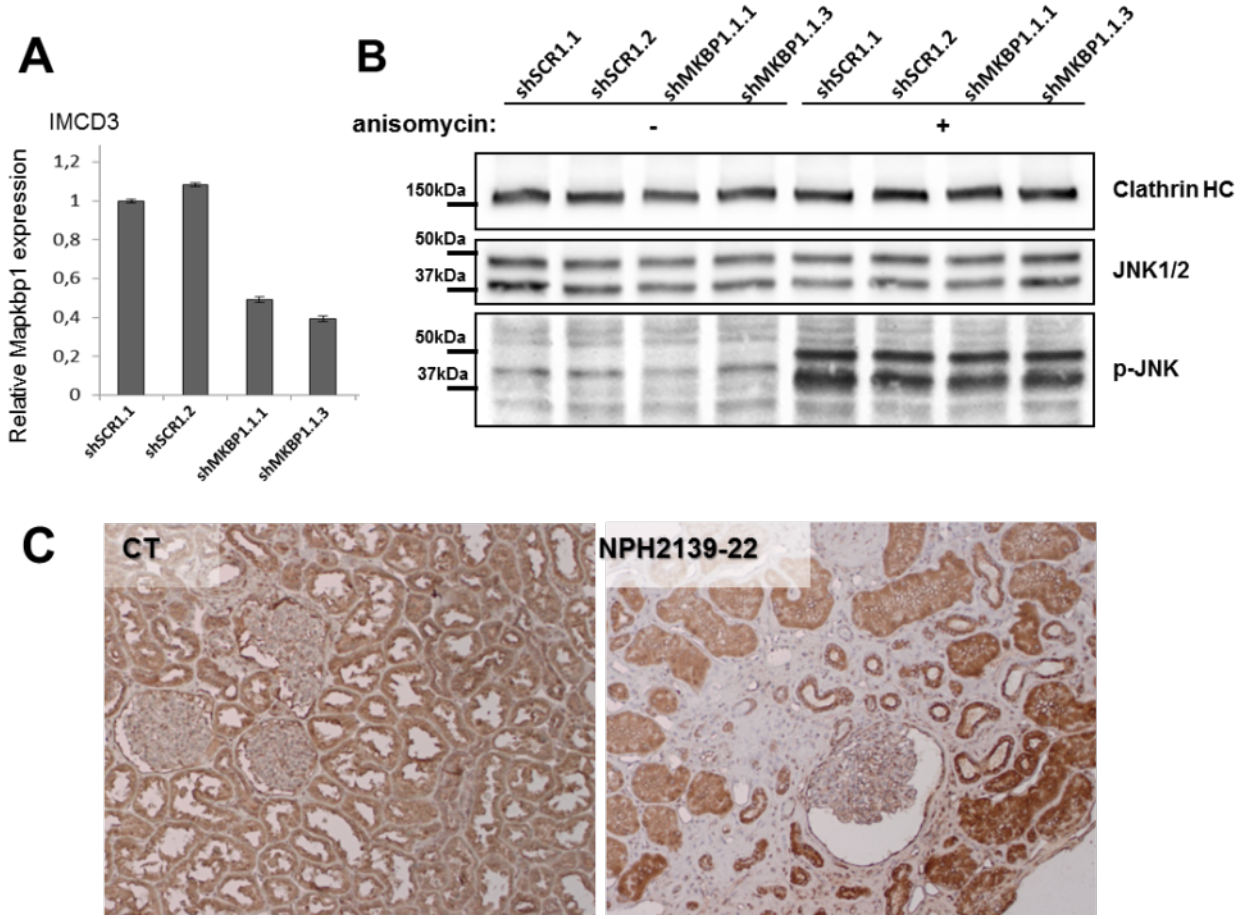

Figure S16: JNK signaling is not altered in *MAPKBP1* mutant conditions.

A) IMCD3 cells were stably transduced by a lentiviral vector (pLKO.1-TRC vector; https://www.addgene.org/8453/) expressing either scrambled or *Mapkbp1* (Sh#5: 5'-CCAGTCAACAACCTTCTCCAA–3') targeting shRNA. Expression of *Mapkbp1* (mMKBP1-qPCR-20F: 5'CCAGCTCTGCCCATCCTT-3'; mMKBP1-qPCR-22R: 5'-TCCAGGTACTCCATGGTCTCTTG-3') measured by quantitative RT-PCR was normalized to *Hprt* (mHPRT-qPCR-F: 5'-AGGGCATATCCAACAACAACCTT-3'; mHPRT-qPCR-R: 5'-GTTAAGCAGTACAGCCCCAAA-3') expression in both control (shSCR1.1, shSCR1.2) and *Mapkbp1* (shMKBP1.1.1; shMKBP1.1.3) IMCD3 clones. **B**) IMCD3 cell lines expressing scrambled or Mapkbp1 targeting shRNA were treated or not with anisomycin (1,25ng/µl) for 1h, then lyzed and analyzed by western-blot using antibodies against clathrin heavy chain (HC, loading control; rabbit polyclonal, Abcam ab21679, dil 1/5000), JNK1/2 (clone 252323, R&D system, 1/5000) or phosphorylated JNK (p-JNK; AF1205, R&D system , 1/5000). **C**) Kidneys from control and from NPH2139-22 individuals with an antibody against phosphorylated Jun (p-c-Jun; 9261S, cell signaling, 1/50).

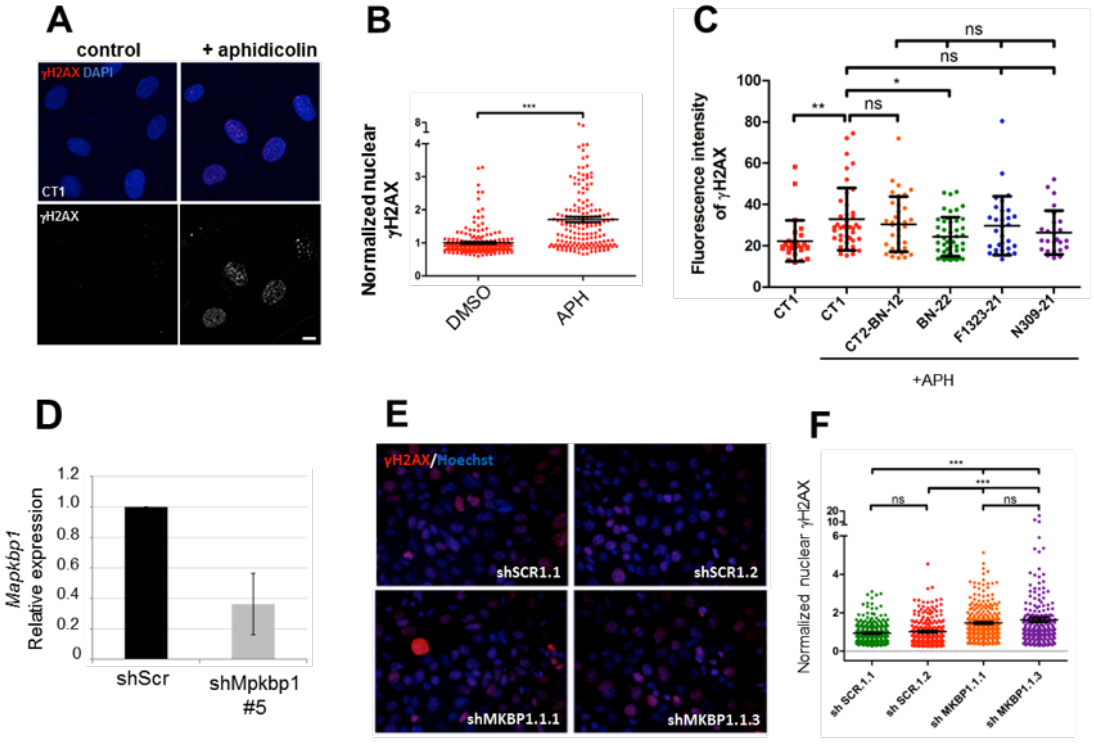

Figure S17: Effect of MAPKBP1 mutations or knockdown on DDR signaling.

(A) Fibroblasts from control individual (CT1) were treated or not with aphidicolin (APH; 400 nM, 24hrs) fixed (PFA) and stained for phosphorylated γH2AX (red; mouse monoclonal, clone JBW301 [MILLIPORE 05-636], 1/200) together with DAPI (blue). **(A)** Intensity of nuclear γH2AX staining was quantified from three independent experiments using imageJ (n: DMSO=233, APH=167). ns and ***p < 0.0001 were calculated via Dunn's Multiple Comparison Test after the analysis of variance ANOVA test. Scale bar, 5μm. (**C**) Fibroblasts from controls and affected individuals were treated with APH fixed and stained for phosphorylated γH2AX and intensity of nuclear γH2AX staining was quantified as in (**A**). One representative experiment out of two is shown (n>25). Ns, *p < 0.01 and **p < 0.001 were calculated via Dunn's Multiple Comparison Test after the analysis of variance ANOVA test. (**D**) Expression of *Mapkbp1* was measured in NIH 3T3 cells clones expressing scrambled (shSCR) or Mapkbp1 (shMapkbp1#5) targeting shRNA (**Figure S16**) by quantitative RT-PCR and normalized to *Gapdh* expression. Error bars indicate s.d., derived from four independent experiments. (**E, F**) IMCD3 cells clones expressing scrambled (shSCR) or Mapkbp1 (shMKBP1) targeting shRNA (**Figure S16**) were analyzed similarly as in **Figure 7**. IMCD3 cells were fixed and stained for γH2AX (red) together with DAPI (blue). The intensity of nuclear γH2AX staining was quantified from three independent experiments (n>220). ns and ***p < 0.0001 were calculated via Dunn's Multiple Comparison Test after the analysis of variance ANOVA test.

Supplementary tables

	F1323-21	A3977-22	BN-22/23	NPH309-21	NPH2139-21
Next generation sequencing	Whole exome				Ciliome
Total variants called	451,846	340,459	18,315	54,781	5,983
Coding and splice site variants excluding synonomous variants	/	/	8,686	14,344	885
rare variants (not in in-house databases or dbSNP132 and 1KG, MAF<0.5%)	1,680	2,275	232	188	32
Linkage analysis (Figure S1)	170	142	/	6	/
Quality filtering ; Compound heterozygote or homozygote variants (recessive disease model)	/	/	10	1	3
Surviving variants to evaluation	24	15	10	1	1

Table S1: Candidate gene selection from whole exome or ciliome resequencing in affected individuals. The number of variants that remained after filtering strategy (see below for each family), are shown for each individual. A quality filter was applied for all variants: all calls with a read coverage ≤ 2 and a Phred-scaled SNP quality of ≤ 20 were filtered out.

For F1323-21 and A3977-21 individuals, WES and variant burden analysis was performed as previously described[5] using Agilent SureSelect human exome capture arrays (Life Technologies) with next generation sequencing (NGS) on an Illumina HiSeq sequencing platform. Sequence reads were mapped against the human reference genome (NCBI build 37/hg19) using CLC Genomics Workbench (version 6.5.1) software (CLC bio). The average coverage was 62 X with 96% of target bases covered at least 10 X. Variants with minor count <2 and with minor allele frequencies <1% in the dbSNP (Version 137) database were selected and annotated for impact on the encoded protein and for conservation of the reference base and amino acid among orthologs across phylogeny. Mutation calling was performed by geneticists/cell biologists, who had knowledge of the clinical phenotypes and pedigree structure, as well as experience with homozygosity mapping and exome evaluation.

For family BN (BN22-BN23), WES was performed at HudsonAlpha Institute for Biotechnology (Huntsville,AL) using Roche-NimbleGen Sequence Capture EZ Exome v2 kit and paired-end 100nt sequencing on the Illumina HiSeq, analyzed with Casava v1.8 (Illumina Inc) and aligned to the hg19 reference genome using Burrows-Wheeler Aligner (BWA) to a total of 74 X median coverage of the target capture regions with more than 93% of target bases covered at least 20 X. Variant calling (coding and putative splice sites) was performed as described elsewhere[6]. Coding variants and variants in putative splice sites were further filtered against variants identified in 300 Norwegian exome-resequencing samples and variants present at >0.5 % allele frequency in the 1000 Genomes database.

For the NPH309-21 affected individual, WES and variant burden analysis was performed as described previously[7]. The raw data FASTQ files were first mapped to NCBI build 37/hg19 reference genome using 'BWA'. Duplicated reads were removed using 'Samtools'. BAM files were processed by Genome Analysis Toolkit (GATK) to make local realignment and base score recalibration. GATK's UnifiedGenotyper module was used to call variants. Run GATK to generate VQSLOD score for each variant. Run VEP to annotate the effect of the variants. The average coverage is 86X. Nearly 6M variants were generated by GATK. ~97.5% of target exome regions have coverage > 10x.

Ciliary exome targeted sequencing and bioinformatics filtering conducted in NPH2139-21 individual was performed using a custom SureSelect capture kits (Agilent Technologies) targeting 4.5 Mb of 20,168 exons (1 221 ciliary candidate genes), including MAPKBP1[4]. Briefly, Agilent SureSelect librairies were prepared from 3 µg of 300 genomic DNA samples sheared with a Covaris S2 Ultrasonicator according to manufacturer's instructions. The Ovation Ultralow System (NuGEN Technologies) was used to prepare HiSeq2500 pre-capture barecoded libraries. The ciliome capture by hybridization was performed on a pool of 10 to 16 barecoded precapture libraries. Sequencing performed on HiSeq2500 (Illumina) was done on pools of barcoded ciliome librairies (16 ciliome libraries per lane of HiSeq FlowCell). Paired-end reads were generated (100+100) and mapped on human genome reference (NCBI build37/hg19 version) using BWA. Downstream processing was carried out with the GATK, SAMtools, and Picard Tools, following documented best practices (http://www.broadinstitute.org/gatk/guide/topic?name=best-practices). All variants were annotated using a software system developed by the Paris Descartes University Bioinformatics platform. The mean depth of coverage obtained was 112x, and more than 91% of the exome was covered at least 30x. A quality filter was applied for all variants: all calls with a read coverage ≤ 2 and a Phred-scaled SNP quality of ≤ 20 were filtered out. Different filters were applied to exclude all variants located in non-exonic regions, pseudogenes, UTRs or known polymorphic variants with a frequency above 1%, i.e. present in databases such as dbSNP, 1000 genome projects and all variants identified by in-house exome sequencing (8445 exomes and 1289 ciliomes).

The functional consequences of missense variants was predicted using SIFT (http://sift.jcvi.org/www/SIFT_enst_submit.html), PolyPhen2 (http://genetics.bwh.harvard.edu/pph2/) and mutation taster (http://www.mutationtaster.org/) softwares.

Table S2 : Overview of bi-allelic variants identified from exome or ciliome data in affected individuals.

Genes written in bold letters indicate likely disease-causative variants. Segregation analysis revealed that *MAPKBP1* variants segregate with disease in these families (shown in the pedigree in Fig.1). Columns from left to right: position of the variant in hg19 (genomic position), chromosome (chr), name of the gene in which the variant is detected (Gene), RefSeq accession, nucleotide (Nt) and amino acid (AA) change, Polyphen 2 (PP2) and SIFT Score (red : predict disease causing, yellow: intermediate, green: predict benign), homozygotes (hom) or heterozygotes (het) variants, number of reads whereby position is covered for reference allele (Ref) and variant allele (var), genes and variants reported in Biobase/HGMD and associated disease, allelic frequency in Exome Aggregation Consortium (ExAC), validation by Sanger sequencing (Sanger), variant segregate with disease (Segregation). [a]Variant does not occur homozygously in ExAC. [b]IDH3B was previously reported to cause Retinitis pigmentosa when defective. However, this association is only based on a single publication with 2 affected families[8].

References:

1. Schuetz, A., Allali-Hassani, A., Martín, F., Loppnau, P., Vedadi, M., Bochkarev, A., Plotnikov, A.N., Arrowsmith, C.H., and Min, J. (2006). Structural basis for molecular recognition and presentation of histone H3 by WDR5. EMBO J. *25*, 4245–4252.

2. Ruthenburg, A.J., Wang, W., Graybosch, D.M., Li, H., Allis, C.D., Patel, D.J., and Verdine, G.L. (2006). Histone H3 recognition and presentation by the WDR5 module of the MLL1 complex. Nat. Struct. Mol. Biol. *13*, 704–712.

3. Cartegni, L., Wang, J., Zhu, Z., Zhang, M.Q., and Krainer, A.R. (2003). ESEfinder: A web resource to identify exonic splicing enhancers. Nucleic Acids Res. *31*, 3568–3571.

4. Bizet, A.A., Becker-Heck, A., Ryan, R., Weber, K., Filhol, E., Krug, P., Halbritter, J., Delous, M., Lasbennes, M.-C., Linghu, B., et al. (2015). Mutations in TRAF3IP1/IFT54 reveal a new role for IFT proteins in microtubule stabilization. Nat. Commun. *6*, 8666.

5. Boyden, L.M., Choi, M., Choate, K.A., Nelson-Williams, C.J., Farhi, A., Toka, H.R., Tikhonova, I.R., Bjornson, R., Mane, S.M., Colussi, G., et al. (2012). Mutations in kelch-like 3 and cullin 3 cause hypertension and electrolyte abnormalities. Nature *482*, 98–102.

6. Haugarvoll, K., Johansson, S., Tzoulis, C., Haukanes, B.I., Bredrup, C., Neckelmann, G., Boman, H., Knappskog, P.M., and Bindoff, L.A. (2013). MRI characterisation of adult onset alpha-methylacyl-coA racemase deficiency diagnosed by exome sequencing. Orphanet J. Rare Dis. *8*, 1.

7. Boyer, O., Woerner, S., Yang, F., Oakeley, E.J., Linghu, B., Gribouval, O., Tête, M.-J., Duca, J.S., Klickstein, L., Damask, A.J., et al. (2013). LMX1B mutations cause hereditary FSGS without extrarenal involvement. J. Am. Soc. Nephrol. JASN *24*, 1216–1222.

8. Hartong, D.T., Dange, M., McGee, T.L., Berson, E.L., Dryja, T.P., and Colman, R.F. (2008). Insights from retinitis pigmentosa into the roles of isocitrate dehydrogenases in the Krebs cycle. Nat. Genet. *40*, 1230–1234.